SHAPE FACTOR ANALYSIS OF GRANULAR FILTER MEDIA AND ITS EFFECTS ON SETTLING VELOCITY AND STRATIFICATION POST-BACKWASH

by

Lindsay Matthy

A thesis submitted to the faculty of
The University of North Carolina at Charlotte
in partial fulfillment of the requirements
for the degree of Master of Science in
Civil Engineering

Charlotte

2016

Approved by:

____
Dr. James Amburgey

____
Dr. Olya Keen

____
Dr. James Bowen

ABSTRACT

LINDSAY MATTHY. Shape factor analysis of granular filter media and its effects on settling velocity and stratification post-backwash. (Under the direction of DR. JAMES AMBURGEY)

Research on irregularly-shaped granular filter media has been sparse. Previous studies attempted to identify a common shape factor and incorporate it into settling velocity models for spherical media. This common shape factor was frequently called sphericity. However, the use of a sphericity factor results in inaccurate calculations of the actual particle diameter and surface area due to the irregular nature of particles. Through this research, the shape of granular filter media, anthracite specifically, was analyzed in order to better understand the controlling factors of shape as it relates to settling velocity and stratification post-backwash. Media grains were measured utilizing a three-dimensional, perpendicular axis approach and tested in a zero-flow settling column. It was found that the smallest dimension is the strongest predictor of settling velocity. This is because the drag surface area, or the perimeter surface area of the particle falling parallel to the direction of the fall, changes as this smallest dimension changes altering the drag forces on the falling particle. Rectangular aluminum bars were employed as model particles to better understand the results seen in irregular-shaped anthracite and confirmed the relationship between the smallest dimension (or height) and settling velocity.

Additionally, it was shown that anthracite does not stratify in the same manner as sand following backwash. Instead, there was significant evidence to support that the settling velocity of anthracite is strongly influenced by shape variations instead of a single size measurement, whereas the settling velocity of sand was more strongly

controlled by size since there was significantly less variation in the shape of these grains. When comparing stratification of anthracite to sand, anthracite only showed stratification of 10-15% of the total number of grains in the filter column while sand showed 91% stratification.

DEDICATION

This work is dedicated to my supportive mom and dad who have always encouraged this venture. I would also like to dedicate this work to my amazing boyfriend Chris Diaz who has been there with me through every step of this process and has consistently pushed me to achieve my goals as well as my loyal and loving friends Christine Ripley, Kendall Walsh and Heather Piercy.

ACKNOWLEDGMENTS

I would like to thank my advisor, Dr. James Amburgey, for all of his time and guidance through the duration of this research. I would also like to thank the other members of my committee, Dr. Olya Keen and Dr. James Bowen for their time and contribution. In addition, I would like to thank Derek French of Wateropolis Corp. for his time, interest and insight into my work.

And a special thank you to Wateropolis Corp. for providing ceramic and low density anthracite media samples, as well as Red Flint Sand and Gravel for providing sand, and Best Sand & Gravel for providing anthracite. The assistance of Ted Brown in the CEE Machine Shop was also very valuable in producing the aluminum pieces used in the settling column experiments.

TABLE OF CONTENTS

LIST OF FIGURES

LIST OF TABLES

CHAPTER 1: INTRODUCTION

1.1 Background

Current practice predicts the behavior of filter media during and after backwash based on size, bulk density, and porosity properties of the media (Epstein and Pruden, 1999). Particle shape has been proposed as a predictive factor for the settling velocity of natural, irregularly shaped particles. Stokes' Law, an equation used to predict the settling velocity of a true sphere, was developed in 1851 and has been utilized in the prediction of falling spherical particles, but Stokes' Law becomes less useful as particles deviate from a spherical shape (Bagitto and Tsouris, 2008).

$$v_s = \frac{g(\rho_S - \rho)d_p^2}{18\mu} \qquad (1)$$

Where v_s is settling velocity, μ is absolute viscosity, g is acceleration due to gravity, ρ_s is density of a sphere, ρ is fluid density and d_p is equivalent sphere diameter.

Researchers have attempted to develop models that would alter Stokes' Law to account for the irregular shape of most naturally-occurring particles. Several "shape factor" models have been developed, but many of these shape factors were developed using isometrically shaped particles and were difficult to fit to naturally occurring irregular particle shapes (Baba and Komar, 1981). Many sources called for additional research on shape factor for non-spherical particles over the last 35 years, yet research is still lacking. While rules-of-thumb have been used in practice for dual media filters of sand and anthracite for the prediction of settling and intermixing, these rules have shown ineffective when applied to other media interfaces (Hudson Jr., 1938; Kawamura, 1975). In order to increase the overall efficiency of filter performance, the introduction of other filter media such as low-density crushed ceramic has been proposed as a tri-media layer above anthracite (French, 2012). Tri-media filters improve filter performance by increasing filter run times, and lowering filtered water turbidity (Amburgey and Brouckaert, 2011). Studies employing these rules-of-thumb and current settling models found that the ceramic would significantly sink into the anthracite layer due to changes in the ceramic density over time since the high porosity of the ceramic allows for the uptake of water (Amburgey and Brouckaert, 2011; Tassitino, 2014).

Additional research into shape factor is necessary to understand these settling velocity and interface relationships for the purpose of optimizing filter performance. Additionally, no previous research defined or analyzed how shape factor affected stratification and/or fluidization in a conventional filter other than hinting at possible correlations. To add to the need for additional research is the lack of published results on anthracite with most research focusing on naturally occurring rocks and quartz sand.

This document reports an in-depth analysis of anthracite shape, settling velocity and stratification. A three-dimensional perpendicular axis approach is commonly used in other shape factor analyses. With this approach, it is possible to single out each dimension and find individual relationships to particle settling behavior. Irregular particles have been shown through this research to orient during settling with their smallest dimensions parallel to the fall direction.

1.2 Objectives

This research project had the following objectives:

- Analyze filter media, anthracite specifically, in terms of shape factor and sphericity to better understand mixing behavior of anthracite and a second, less dense ceramic layer.
- Define shape factor and determine how filter media layers stratify during fluidization.
- Develop a mathematical model to predict settling velocity of filter media.
- Determine the aspects of shape factor that govern settling and stratification through particle dimension analysis and the analysis of drag forces

CHAPTER 2: LITERATURE REVIEW

2.1 Sphericity

Research into irregularly shaped particle characteristics and how they affected settling velocity began in the early 1930s most notably when Wadell performed a size classification study of naturally occurring rocks. Through his research, he found that shape and volume, while both important factors are not dependent on one another (Wadell, 1932). This finding highlights the interesting distinction between shape and size. Wadell stated that size was expressed as a volume term and that shape was irrelevant in size determination, however shape can vary both the size and the volume making it difficult to define. He proposed that it was necessary to determine a single common shape factor to standardize and compare values of settling particles. From this he developed the shape factor of sphericity (ψ) shown in Equation 2

$$\psi = \frac{A_s}{A_p} \qquad (2)$$

with A_s representing the surface area of a sphere of equivalent volume, and A_p representing the actual surface area of the particle. A sphericity value of 1 indicates a true sphere. Equation 2 highlights the importance of sphericity in the use of settling velocity equations by showing that the lower the sphericity, or greater deviance from a true sphere, settling velocity of that particle decreases due to increased surface area (i.e. shape change), but the settling velocity changes with no change in volume or mass (Wadell, 1932). Challenges arise in determining the true surface area of non-spherical particles because of the use of the nominal diameter, the diameter of a sphere of equivalent volume, in determining the volume of the irregularly shaped particles (Wadell, 1932). Additionally, other researchers have suggested that sphericity/shape factor alone is not a strong enough predictive factor in terms of settling velocity and stratification of dual media filters (Escuidé et al., 2006).

2.2 Other Shape Factors

Bagitto and Tsouris (2008), described shape factor as the, “ratio of characteristic parameters [volume, surface area, projected area and projected perimeter] to the corresponding value for the equivalent sphere.” Research has shown that the settling velocity of non-spherical particles is lower than spherical particles (Goldbery and Richardson,1989). This is due to the greater displacement around the irregularly shaped particle as it is falling because of a higher surface area creating increased drag forces (Deitrich, 1982). Yet, the degree to which shape is affecting settling velocity is still not fully understood (Goldbery and Richardson, 1989). Throughout the last 80 years, researchers have attempted to develop a standard shape factor and use it to accurately predict the settling velocity for non-spherical, irregularly-shaped particles. One research study was successfully able to show that shape has an influence over stratification by testing particles of varying shapes while holding volume and density constant (Escuidé et al., 2006).

2.2.1 Shape Factor and Settling Velocity Models

Several shape factors have been developed. Most notably are sphericity, the Corey shape factor (CSF), and the Janke shape factor (E). The CSF was developed in 1949 following difficulty of the use of sphericity for the reasons mentioned in the previous section relating to the measurement of an irregular particle’s surface area (Komar and Reimers, 1978). The CSF, unlike sphericity, is a relationship between a particle’s own axial dimensions rather than a ratio of surface areas making it easier to use

$$CSF = \frac{D_s}{\sqrt{D_i D_l}} \qquad (3)$$

where D_s is the smallest diameter, D_i is the intermediate diameter, and D_l is the largest diameter (Komar and Reimers, 1978). In a study conducted by Komar and Reimers using ellipsoidal pebbles, they found that the CSF was a better predictor of settling velocity and drag as they relate to shape than did sphericity (Komar and Remiers, 1978). An adapted form of the Stokes’ Law equation was developed to create curves for different CSF values to predict settling velocities

$$v_s = \frac{(\rho_s - \rho) g D_l^2}{18\mu(0.956 CSF^{-0.378})} \qquad (4)$$

$$v_s = \frac{(\rho_s - \rho) g D_l^2}{18\mu(2.18 - 2.09(CSF))} \qquad (5)$$

where D_l is the nominal diameter. Equation 4 is used for 0.4≤CSF<0.8 and Equation 5 for CSF<0.4 (Komar and Reimers, 1978). Issues with this formula arise from the empirical nature of having to develop multiple curves to account for each CSF value. Additionally the larger the D_L, the less predictive Equation 4 becomes (Komar and Reimers, 1978). This leaves the equation most useful only for small grain particles such as sand (Komar and Reimers, 1978).

The Janke shape factor, E, was developed in 1966 and again utilized a three dimensional axis approach to define shape.

$$E = \sqrt{D_s\left[\frac{D_l^2+D_i^2+D_s^2}{3}\right]} \quad (6)$$

This shape factor is more complex than the Corey shape factor and has therefore not been a preferred tool for measuring particle shape (Dietrich, 1982). However, it eliminates the need for multiple curves for settling velocity prediction with the use of Equation 6 (Dietrich, 1982).

$$v_s = \frac{(\rho_s-\rho)gD_n^2E^{0.28}}{18\mu} \quad (7)$$

Because of the complex nature of the Janke shape factor, it is more commonly used to calculate the settling velocity for axisymmetric shapes such as cylinders and ellipsoids (Baba and Komar, 1981).

2.2.2 Drag Coefficient and Reynolds Number

Drag coefficient, a non-dimensional number related to the drag on the surface area of a falling particle, has been an important factor in settling velocity prediction (Deitrich, 1982). Dietrich (1982) noted that most previous research had used drag coefficient and Reynolds number to develop a correlation curve, which can be used to predict a settling velocity. However these correlations are difficult to compare across studies and are generally only applicable to a single analysis (Deitrich, 1982). Reynolds number changes with settling velocity, which it is being used to predict. Additionally, Deitrich thought the continual adjustment and refinement of these curves was of little importance (Dietrich, 1982).

2.3 Minimum Fluidization Velocity and Expansion

Minimum fluidization velocity is an important parameter in backwashing because it is the junction between settled and fluidized states (Amirtharajah and Cleasby, 1972). Several methods for determining the minimum fluidization velocity such as the Kozeny, Richardson and Zaki, Camp, and Wen and Yu expansion models exist (Amirtharajah and Cleasby, 1972). Amirtharajah and Cleasby provided an extensive review of available methods and noted that little research has been conducted since the 1930s on this subject. They also stated that because of the size distribution of particles in a filter system and other particle effects, it is difficult to predict an exact minimum fluidization velocity (Amirtharajah and Cleasby, 1972).

Optimal backwash expansion is at a rate above minimum fluidization velocity where the filter bed is expanded, yet head loss remains constant (Cleasby et. al, 1977). This is because drag forces are responsible for filter cleaning (Cleasby et. al, 1977). A filter bed was defined as fully fluidized at an expansion of 20-50% above the settled bed height (Cleasby et al, 1977).

2.4 Stratification and Intermixing

Cleasby also found that in mono-media rapid sand filters that the sand grains stratified following backwash. This gradation settles the finest particles on the top most layers and largest particles on the bottom of the filter. However, research by Baldock and coworkers was able to show that high concentrations of particles, such as media in a filter bed, tend to have a more uniform distribution (Baldock et al., 2004). This is because particle interactions in a filter hinder settling velocity from that of single particles settling in laminar conditions such as Stokes' Law (Baldock et al., 2004). Richardson and Zaki (1954) developed an equation to account for this hindered settling velocity

$$\frac{v_s}{v_t} = \varepsilon^n = (1-c)^n \quad (8)$$

where v_t is the terminal velocity, ε is porosity v_s is the settling velocity at porosity ε, c is the volumetric concentration, and n is an empirical number based on Reynold's number (Tomkins et al., 2005). For this study, empirical values of n were determined through experimentation with spheres (Baldock et al., 2004).

The addition of a second, less dense, yet larger particle size media above the sand layer provided greater efficiency in filter performance (Cleasy and Woods, 1975; Vigneswaran and Mazumdar, 1984). Due to size and density differences between the two medias, the layers remain separate following fluidization and settling (Cleasby and Woods, 1975). However, the selection of these sizes and densities is largely based on rules-of-thumb empirically determined in a laboratory setting or visually (Cleasby and Woods, 1975). These rules-of-thumb, incidentally, are only useful for a small range of backwash rates and media (Cleasby and Woods, 1975). In order to prevent intermixing of dual media filter layers, size ratios based on specific gravity must be maintained (Conley and Camp, 1961). Because of this, grain size for anthracite is recommended to be 2-3 times larger than sand (Conley and Camp, 1961). An equation was developed by Vigneswaran and Mazumdar (1984) to predict the intermixing ratio

$$L_M = 5.47\left(\frac{d_a}{d_s}\right) - 11.36 \quad (9)$$

where L_M is the intermix length, d_a is the anthracite effective size, and d_s is the sand effective size.

Wen and Yu developed an expansion correlation that predicted intermixing for anthracite and sand sizes with diameter ratios of less than 1.3:1 and stratification for diameter ratios greater than 1.3:1 for a particular d_i (Amirtharajah and Cleasby, 1972; Kawamura, 1999). An empirical relationship can be used for dual-media filters to ensure similar settling velocities using Equation 10

$$\frac{d_1}{d_2} = \left(\frac{\rho_2 - \rho}{\rho_1 - \rho}\right)^{0.667} \quad (10)$$

where ρ_1 is the density of media 1, ρ_2 is the density of media 2, ρ is the water density, d_1 is the effective size of media 1, and d_2 is the effective size of media 2 (Kawamura, 1999).

2.5 Effective Size and Uniformity Coefficient

Sieve analysis is a process that is used to determine the size profile of a graded material (Crittenden et al., 2012). By passing a media sample through different sized cylindrical mesh pans, one can determine the size breakdown of that sample (Crittenden et al., 2012). Current practice relies on the effective size, or d_{10} size, as well as the uniformity coefficient to characterize media. The d_{10} size is representative of the 10 percent smaller media diameter size by weight and the uniformity coefficient (UC) is calculated by dividing the d_{60}, or 60 percent smaller diameter by weight, by the d_{10} (Crittenden et al, 2012). As uniformity coefficient deviates from 1, so too does the uniformity of the media sample. Some questions have been brought up as to the effectiveness of sieve analysis in determining uniformity coefficient and effective size for non-spherical particles. This is because the sieve size is representative of a sphere diameter but is not true of irregularly-shaped particles (Crittenden et al., 2012). For irregularly-shaped particles, the assumption is made that they pass through sieves according to the "largest dimension of the smallest particle cross section" as shown by the dashed line in Figure 1 (Crittenden et al., 2012). Additionally, research has shown that the equivalent sphere diameter assumed for sieve analysis is slightly larger than true media sizes (Cleasby and Woods, 1975). In short, this means that for non-spherical, irregularly-shaped particles sieve analysis is based on both particle size and shape.

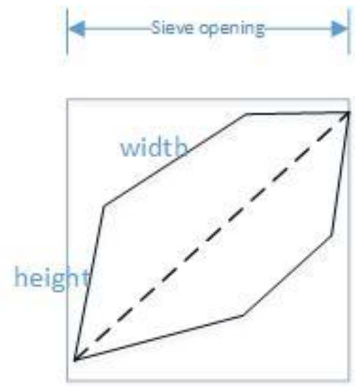

Figure 1: Diameter of smallest particle cross section orientation through a sieve mesh

CHAPTER 3: METHODS

3.1 Density

Density was determined volumetrically (ASTM C128-12). Media samples were soaked for 24 hours then allowed to air dry (saturated surface dry). Once samples dried, a cone test was performed to ensure that the media was saturated surface dry. The sample was then introduced into a volumetric flask filled with water and the change in water volume was recorded. Density of the media sample was then able to be calculated based on the following calculation

$$D\left(\frac{g}{cm^3}\right) = \frac{997.5(W_S)}{V_2 - V_1} \quad (11)$$

where D is density, W_s is the mass of the sample, V_1 is the volume before sample addition, and V_2 is volume after sample addition.

3.2 Sieve Analysis

Sieve analyses were performed using eight-inch stainless steel sieves with mesh numbers 10, 12, 14, 16, and 20 for anthracite and 20, 30, 35 and 40 for sand in accordance with the procedures set forth by the American Society of Materials Testing (ASTM Method C136). One-hundred gram media samples were used in all sieve analyses. Pans were weighed and recorded prior to sieving using an Ohaus Ranger scale to the ±0.1g. The stacked sieves and 100 gram media sample were secured into an orbital sieve shaker (Gilson model SS-15) and allowed to sieve for 5 minutes. Following the sieving, each pan was weighed to determine the amount of media retained.

To calculate the uniformity coefficient, the cumulative percent smaller media was calculated for each sieve and graphed on a semi log plot. This should yield a straight line from which the d_{10} and d_{60} sizes can be determined as shown in Figure 2 using the linear equation. Uniformity coefficient is defined as the d_{60} size divided by the d_{10} size. The d_{10} size, also referred to as the effective size, represents the 10% finer (by mass) size or diameter. As the uniformity coefficient approaches 1, the media becomes more uniform.

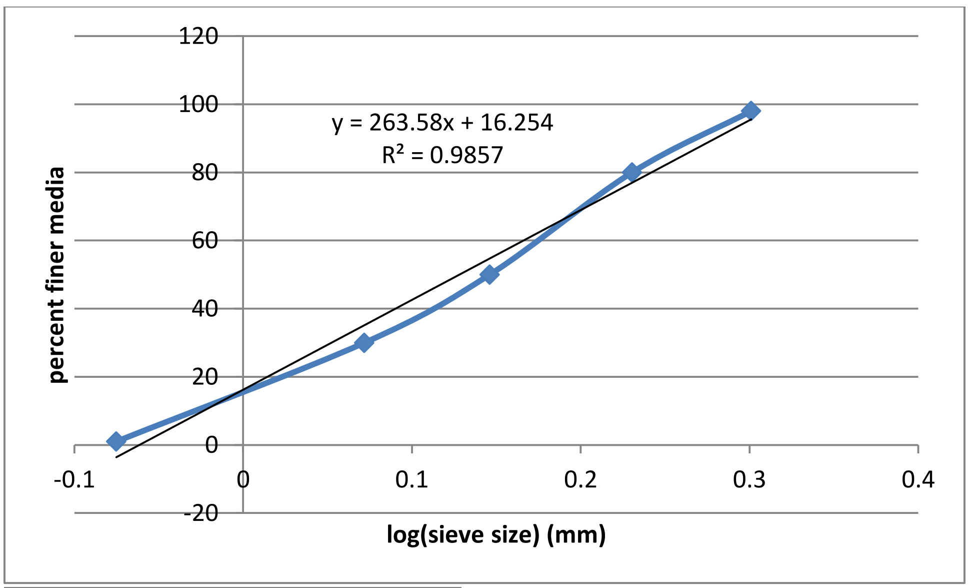

d_{10}	1.10
d_{60}	1.47
UC	1.3

Figure 2:Sieve analysis semi-log plot and calculations

3.3 Pilot Scale Filter Set-Up

Most experiments were carried out using a 2-inch diameter, 72-inch long schedule 40 clear PVC pipe filter column with an IMS cap (Leopold/Xylem, Zelienople, PA) underdrain. Water was pumped through the filter column using an ATB Speck Pumpen centrifugal pump (model AF 63/2C-7) with a recirculation tank to collect and control the temperature of the backwash water. The pump was controlled by a variable frequency drive (Lenzene Americas SMVector, model ESV751N01SXC). Flow rates were monitored using two different flow meters (Krohne IFS electromagnetic flow meter, model IFS4000F/6DIV1, and Krohne, Optimass MFS7000 Coriolis flow meter). Unless otherwise stated, all experiments were carried out with 24 inches of media in the filter column. Media was cleaned through backwashing and skimming prior to use to remove fine particles and simulate typical drinking water filtration practices.

3.3.1 Four-Inch Filter Column

Some experiments were also carried out using a 4-inch diameter, schedule 40 clear pvc filter column also with a Leopold/Xylem IMS cap underdrain. The purpose of this experiment was to determine if there were any wall effects contributing to the results of the 2 inch filter column.

Figure 3: Pilot scale filter configuration

3.4 Backwash Procedure

All filter media samples unless otherwise stated were expanded to 50% and allowed to backwash for 20 minutes. The purpose of expanding the beds rather than calculating a minimum fluidization velocity was to prevent bias by any error in the minimum fluidization rates. By expanding the bed by 50%, it ensured full fluidization of the filter media regardless of calculated and actual minimum fluidization velocities.

3.5 Separation of Media Post-Backwash

Following backwash, the filter column was drained, the column was removed from the stand and the media was removed as a wet plug. Since all backwash tests used 24 inches of media, this method allowed for the separation of the filter column into four 6-inch sections, which were then used in settling velocity analyses. Figure 4 shows a diagram of the filter sections with 1 representing the topmost 6-inch filter section, and 4 representing the bottommost 6-inch filter section.

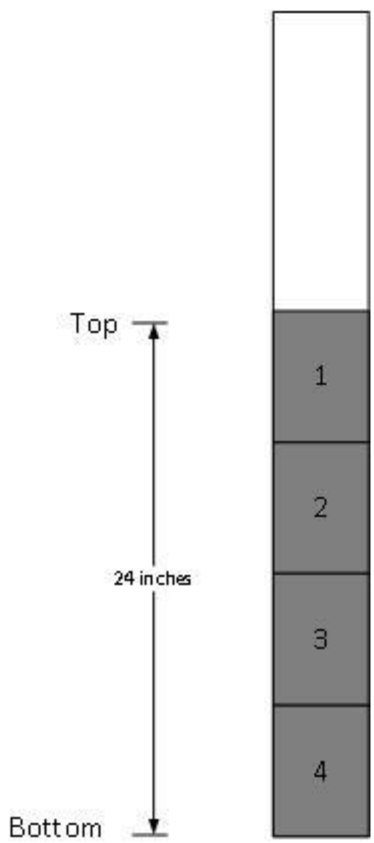

Figure 4: Diagram of 6-inch filter sections

3.6 Settling Velocity Analysis

Settling velocity analysis was carried out in a temperature-controlled room in a 12-inch diameter cylindrical column with water that was kept at 20-21° C under no-flow conditions. A one meter length was marked on the column to be able to calculate settling velocity and a distance above the one meter mark was provided to allow media grains to reach terminal velocity. Thirty grain samples were randomly selected from each section of the filter column. Each media grain was weighed in grams using a Denver Instrument Summit Series balance, model SI-114. Measurements were recorded to the nearest ±.0001gram.

Additionally, each media grain was measured on 3-dimensional axes of length, width, and height perpendicular to each other. For the purpose of this research, height represents the smallest dimension and length represents the largest dimension. These dimensions were measured to the ±0.01 millimeter using a digital caliper.

Following weighing and measuring, media grains were dropped individually into the settling column. An acceleration zone above the one meter mark allowed for grains to reach terminal velocity. Once the media grain reached the one meter mark, drop time was recorded manually using a stopwatch to the ±0.01 second. When the media reached the bottom of the meter length, timing was stopped and the settling velocity was calculated and recorded.

3.7 Drag Surface Area

Drag surface area is the surface affected by drag forces. This was calculated using Equation 12

$$A_{drag} = 2(l * h) + 2(w * h) \qquad (12)$$

where l, w, and h represent length, width, and height respectively, with a level of error due to the irregular shape of the media particles.

3.8 Sphericity

Sphericity was determined for anthracite media particles using Equation 2. Surface area and volume of the media particles were estimated by multiplying the 3 dimension measurements with some systematic error due to irregular grain shapes. From these dimensions, the diameter of a sphere with an equivalent volume could be calculated in order to calculate the surface area of an equivalent sphere.

Calculated settling velocity was tested against measured settling velocity using equation 13, 14 and 15 iteratively,

$$v_s = \frac{4gd_h(\rho_s - \rho_w)}{3C_d\rho_w} 0.5 \qquad (13)$$

$$\psi d = d_h \qquad (14)$$

$$Re = \frac{\rho d_h v_s}{\mu} \qquad (15)$$

where d_h is the diameter of an equivalent sphere, C_d is the drag coefficient, ψ is sphericity, g is force due to gravity, ρ_s is the media density, ρ_w is the water density, and μ is dynamic viscosity (Broukheart and Amburgey, 2011).

3.9 Aluminum Bars

The purpose of introducing aluminum rectangular bars into the research was to create a model for regular shaped (rectangular) particles and to develop a more clear understanding of how shape factor affects settling velocity.

3.9.1 Aluminum Testing Procedure

Settling velocity of the aluminum pieces was determined by releasing the aluminum bars individually into the cylindrical settling column and timed using a stop watch as in the procedure previously described for anthracite samples. The aluminum bars were released into the water with their largest projected surface area facing parallel to the bottom of the cylinder since for the most part this is the orientation aluminum bars went to when dropped.

3.10 Core Sampler Design and Construction

A core sample from the Mt. Holly Water Treatment plant was collected in order to compare stratification in the pilot-scale filters versus full-scale filters. The design for the core sampler was taken from the winner of the 2003 American Water Works Association Gimmicks & Gadgets contest. The Central Lake County Joint Action Water Agency is credited in developing the design and construction methods of the “Wilson”. The core sampler was constructed using a 2-inch diameter, 8 foot long clear schedule 40 PVC pipe. A 3-inch by 2-inch reducing bushing was attached to one end of the pipe using PVC cement. A 1/8-inch diameter 316 stainless steel welding rod was inserted into a tennis ball creating a loop and a nylon rope was tied to this loop. The nylon rope was then pulled through the PVC pipe which served as the plugging mechanism for the sampler. A wooden broom handle was duct taped to the end of the sampler in order to extend the length so that it would reach the media in the filter when inserted from above the fluidized filter bed.

The core sampler is designed to capture filter media from a fluidized bed. During a filter backwash, the core sampler is pushed straight down into the filter with the nylon rope loose to allow the tennis ball to dangle. Once media had entered into the sampler, the rope was pulled tight securing the tennis ball into the bushing cap at the end of the sampler. The bushing has a concave rounded shape which allows the tennis ball to fit into it acting as a plug for the sampler trapping the media but still allowing for water to drain out once the sampler is pulled from the water.

3.10.2 Core Sampler Settling Velocity Testing

Approximately 28 inches of filter media was collected (versus a total anthracite and sand depth of 29 inches) in the core sampler capturing the full anthracite layer and most of the sand/intermix layer. The core sampler was dumped out as a plug and was broken up into sections (top, middle, bottom, intermix layer). Each section of the core sample was tested using the same settling velocity testing procedures described previously in Section 3.6.

3.11 Low Density Anthracite and Ceramic

Wateropolis Corp, a company dedicated to testing and development of granular filter media provided samples of low-density anthracite from the United Kingdom with a specific gravity of 1.43, and a spherical non-expanded ceramic media Ceraflow™. Because of the lower density of the anthracite from the United Kingdom, it allowed for the Ceraflow™ to be placed as a layer below it and due to the difference in densities, the layers remained stratified post backwash. This media was used to aid in the development of my own models and to better understand the effects of intermixing and shape factor in conditions that have already been proven to work successfully.

3.11.1 Minimum Fluidization and Expansion of Low Density Anthracite and Ceramic

A filter column with 12 inches of the Ceraflow-50 and 12 inches of the 0.8mm effective size anthracite was backwashed for 20 minutes at 50% expansion and tested for minimum fluidization velocity and intermixing.

3.12 Minimum Fluidization Velocity of Uniform Anthracite

Anthracite was sieved in order to isolate the media that fell between the 14 and 12 mesh pans (1.4 and 1.7 mm). A 24 inch filter column of this media was backwashed at 50% expansion for 20 minutes first and then tested for minimum fluidization velocity. Minimum fluidization velocity was calculated using Equation 9 (Wen and Yu, 1966)

$$v_{mf} = \frac{\mu\sqrt{1135.69+0.0408Ga}}{\rho_w d_{90}} - \frac{33.7\mu}{\rho_w d_{90}} \qquad (16)$$

$$Ga = \frac{d_{90}^3 \rho_w (\rho_s - \rho_w) g}{\mu^2} \qquad (17)$$

where υ_{mf} is minimum fluidization velocity, and Ga is Galileo number. The uniformity coefficient of this media was assumed to be 1 and therefore the sieve size opening of 1.7 mm was used as the as the d_{90} size in Equation 16 for the minimum fluidization velocity prediction .

CHAPTER 4: RESULTS AND DISCUSSION

4.1 Pilot Filter Core Sample Analysis

4.1.1 Uniformity Coefficient less than 1.5 Anthracite Velocity Profile through the Filter Column

Figures 5, 6 and 7 show the settling velocity profiles from three experiments with 24 inches of 0.95 mm effective size anthracite with a uniformity coefficient of <1.5 (UC <1.5; notated with a less than sign to indicate that the sample has at most a uniformity coefficient of 1.5 and may vary throughout the sample) and a density of 1.57 g/cm^3. Results reflect average settling velocity values and standard deviations based on 30 grains per section. All three figures show similar trends with average values ranging from 0.055 m/s to 0.079 m/s and large overlapping standard deviations in each section. Figure 8 shows the combined settling velocity profile from all three experiments. As can be seen from the figures, there is little to suggest a significant stratification occurring throughout the filter column. Settling velocity average values for Figure 8 range from around 0.062 m/s to 0.078 m/s. Average values do show a slight upward trend from the bottom of the filter to the top. However, standard deviations show significant overlap indicating a lack of uniformity within each section of the filter.

An ANOVA test was performed on the combined data and found P <0.0001 indicating that there was a significant difference between populations which was not expected based on visual representation of the data. To identify where the difference occurred, t-Tests were performed between adjacent sections of the filter. The t-Tests between sections 1 and 2, and 3 and 4 both showed no significant differences with P = 0.099 and 0.052, respectively. Significance was seen between sections 2 and 3 with a P value of 0.0001. A P value is a function of a statistical model that represents how close comparing populations agree with the null hypothesis. Using a significance level of 5%, a P value of $\leq$0.05 indicates that the data does not agree with the null hypothesis and there is a statistical difference. Although the top and bottom halves of the filter show a statistically significant level of difference, it was not to the degree expected. Table 2 provides complete statistical data. Highlighted rows contain results where no significant statistical difference was found.

To quantify the amount (or degree) of stratification occurring, each filter section's mean settling velocity was extended to ±2 standard deviations to provide a 95% confidence interval. From here, media particles that fell within the shaded overlapping range of 0.049-0.091 m/s could be compared against those that fell outside of this range as is shown in Figure 9. Those that fell outside of this range were considered stratified while the remaining particles could have been present in any of the four sections of the filter media. Based on this method, it was found that 87% of the media particles fell within the overlapping range, while only 13% of the media was considered stratified.

The initial hypothesis regarding design of tri-media filter design utilizing low-density ceramic media over anthracite coal was that filter anthracite layer stratified in a manner that would allow for the top section (or lowest settling velocity sections) of the filter column to be preferentially removed in order to add a ceramic layer above the anthracite that would not intermix or sink below the anthracite layer. Because results did not show stratification to the degree expected, it was not possible to simply remove the top section of the anthracite layer to alter the settling velocity and control the degree of intermixing. Therefore, the project goals shifted toward analyzing why filter media do or do not stratify.

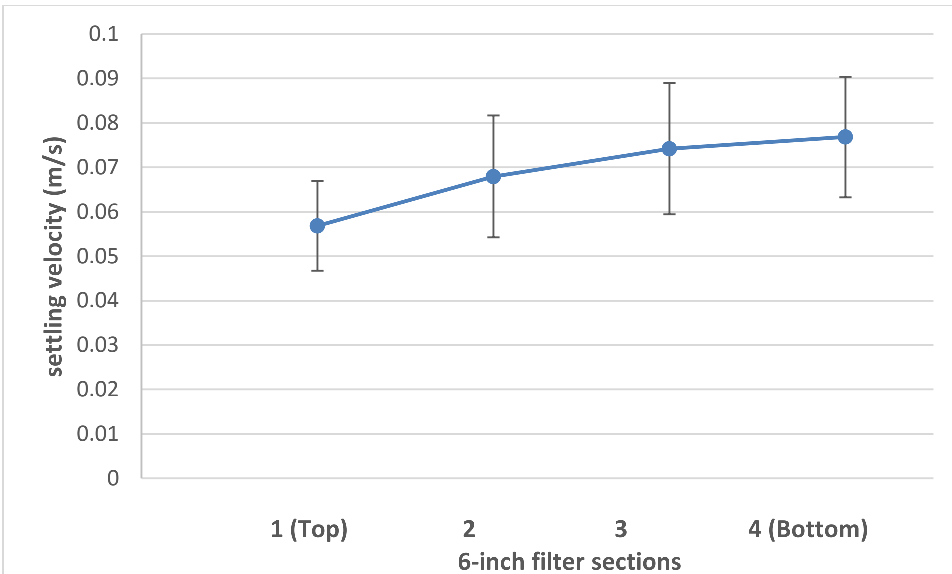

Figure 5: UC <1.5 0.95 mm ES settling velocity profile average values and standard deviation of each 6-inch filter section from experiment 1

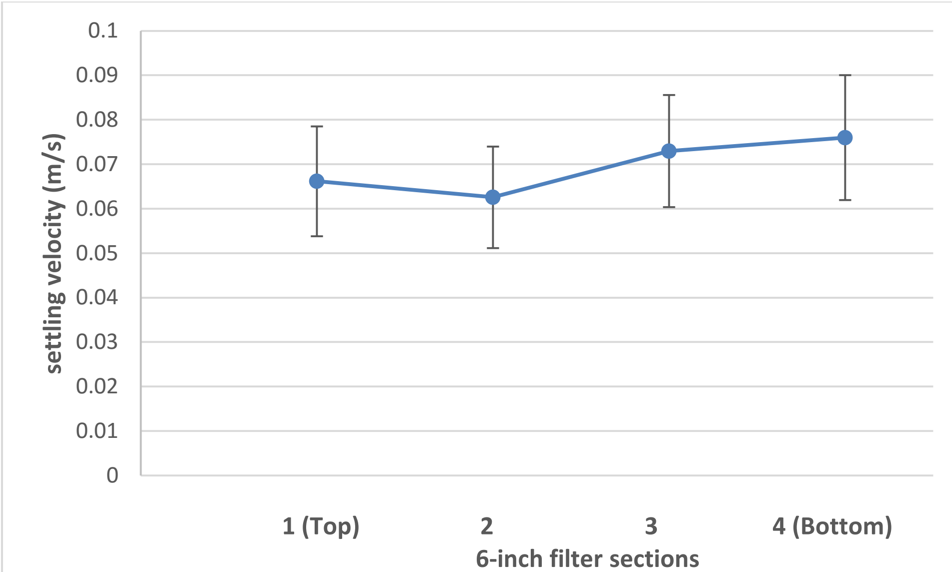

Figure 6:UC <1.5 0.95 mm ES settling velocity profile average values and standard deviation of each 6-inch filter section from experiment 2

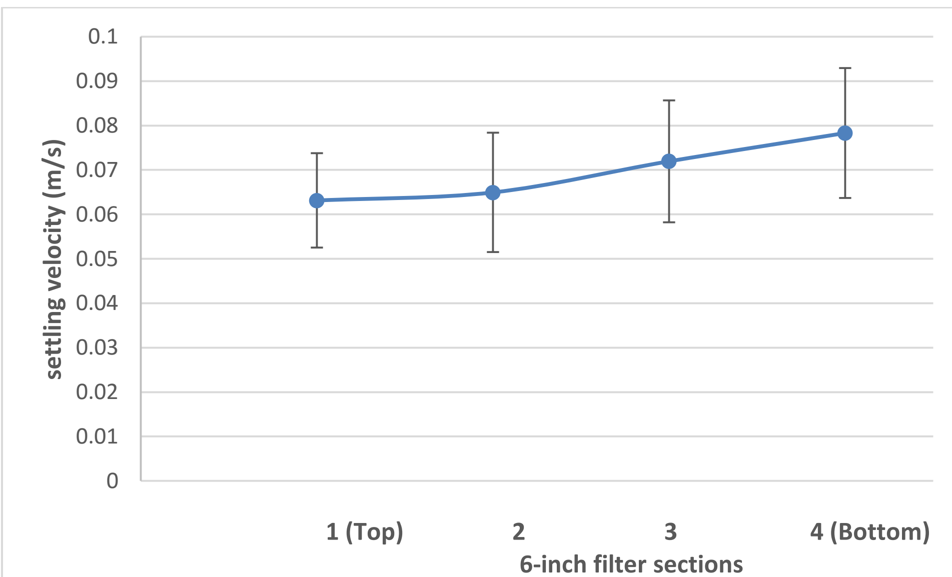

Figure 7: UC <1.5 0.95 mm ES settling velocity profile average values and standard deviation of each 6-inch filter section from experiment 3

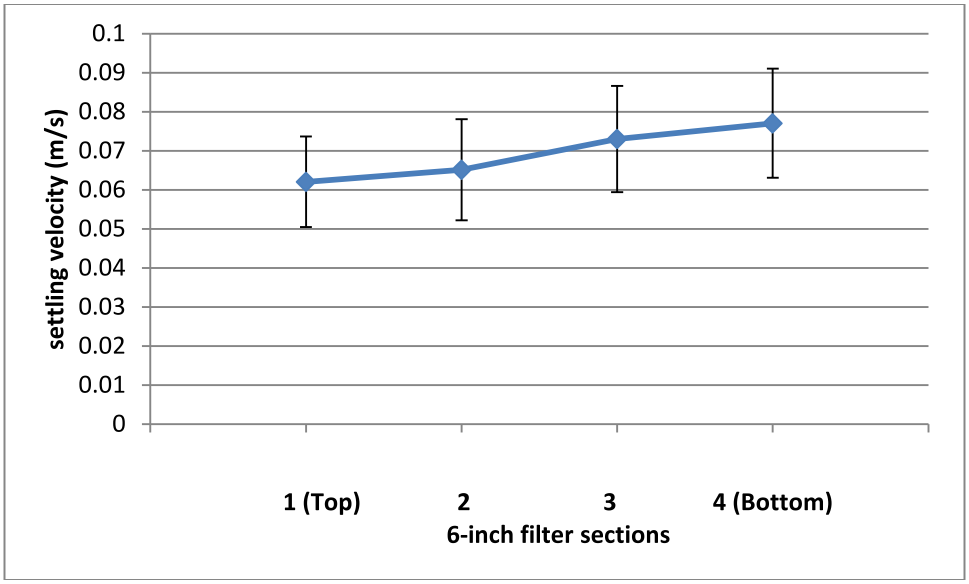

Figure 8: UC <1.5 0.95 mm ES combined anthracite velocity profile average values and standard deviation of each 6-inch filter section from three filter column tests

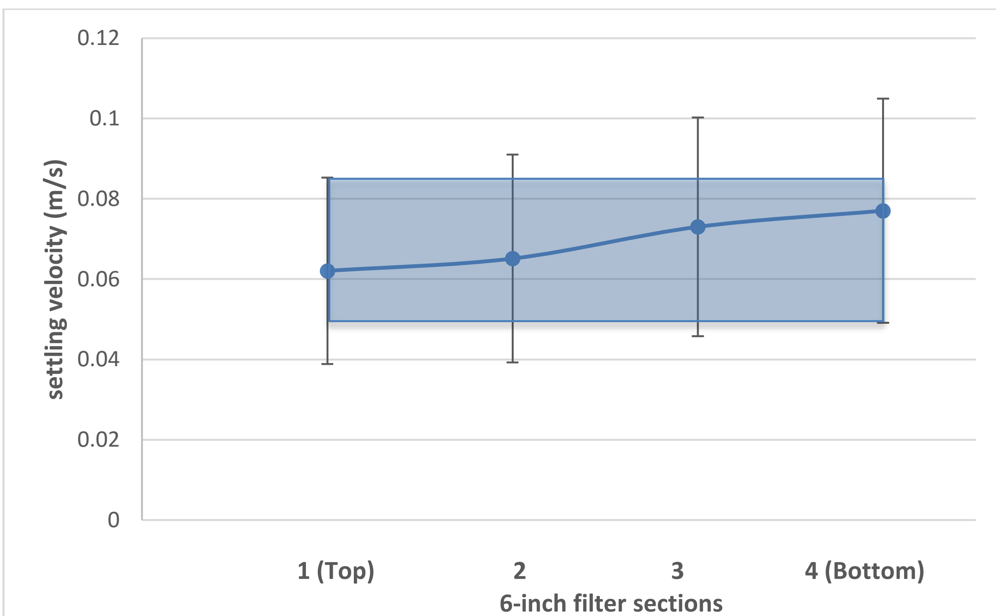

Figure 9: Stratification diagram with 95% confidence interval of UC <1.5 media

Table 1: Statistical comparison of filter sections settling velocity for combined anthracite settling velocity data

t-Test section comparisons	**P value of anthracite filter sections settling velocity**
1 and 2	0.099
1 and 3	<0.0001
1 and 4	<0.0001
2 and 3	0.0001
2 and 4	<0.0001
3 and 4	0.052

4.1.2 Ramp Down of Backwash Flow versus Direct Shutoff for Anthracite Filter Columns

Figure 10 shows settling velocity results from a filter column experiment that had backwash flow immediately shut off following the 20 minute backwash at 50% expansion; while Figure 11 shows settling velocity results from a filter column test that was ramped down in approximately 25% increments every 5 minutes for 20 minutes. Figure 11 max velocity was 34 gpm/ft^2 (86 m/h) at 50% expansion and ramped down to 28, 22, 16 and 11 gpm/ft^2 respectively over the 20 minute period. Looking at Figures 10 and 11, there is not a large noticeable difference between the velocity profiles. Based on these results, ramp down speed seemed to add no effect on the stratification and settling of the anthracite media in the filter post backwash. To confirm this, t-Tests were performed for each section of the filter column for the ramped down filter column against the results of the same section of the direct shut off column. Results found P values to be 0.32, 0.47, 0.77, and 0.53 for sections 1, 2, 3, and 4 respectively indicating there is no statistical difference in settling velocity profiles between flow reduction methods.

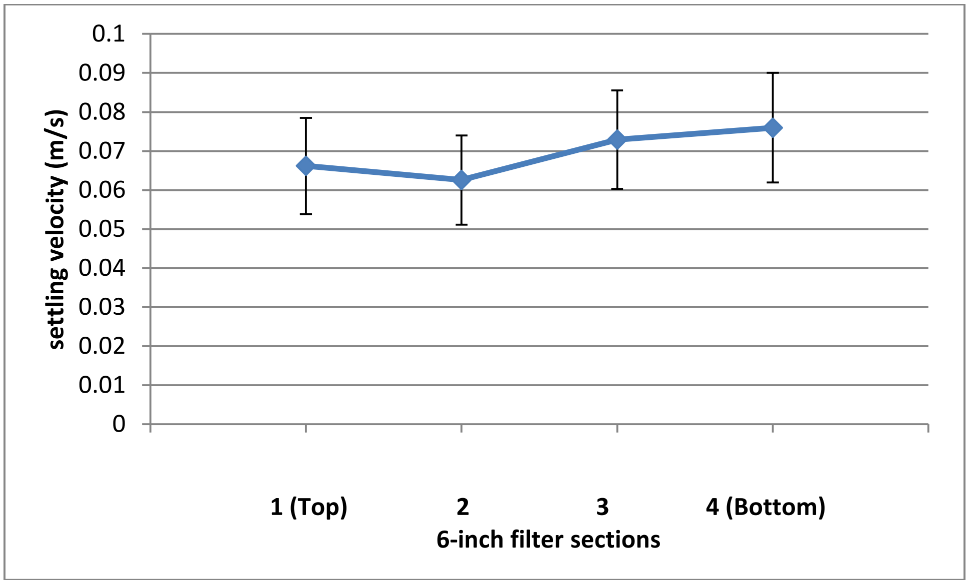

Figure 10: Settling velocity profile of anthracite backwash test with flow immediately shutoff

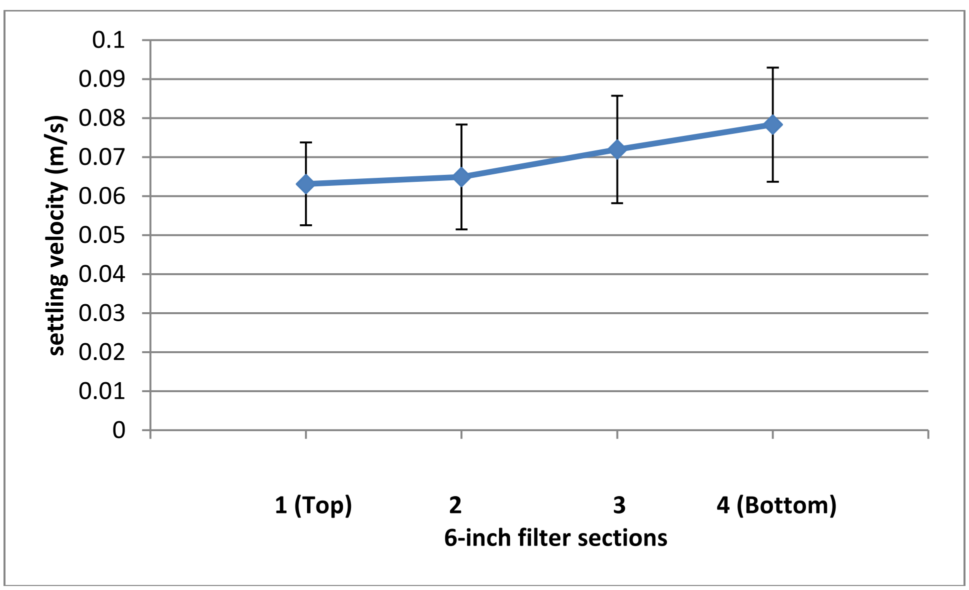

Figure 11: Settling velocity profile of anthracite backwash test with flow ramped down in 25% increments over 20 minutes

4.1.3 Uniformity Coefficient less than 1.6 Anthracite

4.1.3.1 Velocity Profile through the Filter Column

A 1.10 mm effective size, uniformity coefficient <1.6 (UC <1.6) media was used to further study stratification within the filter. The initial hypothesis was that with a higher uniformity coefficient there would be a greater variation in the media, which would yield a stronger stratification profile from the top of the filter through the bottom. From Figure 12, it is evident that uniformity coefficient was not a strong factor in stratifying the bed. In fact, the results of the higher uniformity coefficient media appear even less stratified than the <1.5 UC media. An ANOVA test confirmed the null hypothesis with a P value of 0.094 indicating that there is no significance between the four populations.

Additionally, the same method for quantifiying stratification for the lower uniformity coefficent media was applied for this media by comparing individual grain settling velocities to the 95% prediction intervals that overlap. It was found that 91% of the filter media fell within the overlapped area of 0.047-0.110 m/s and only 9% of the media was considered stratified as is shown in Figure 13.

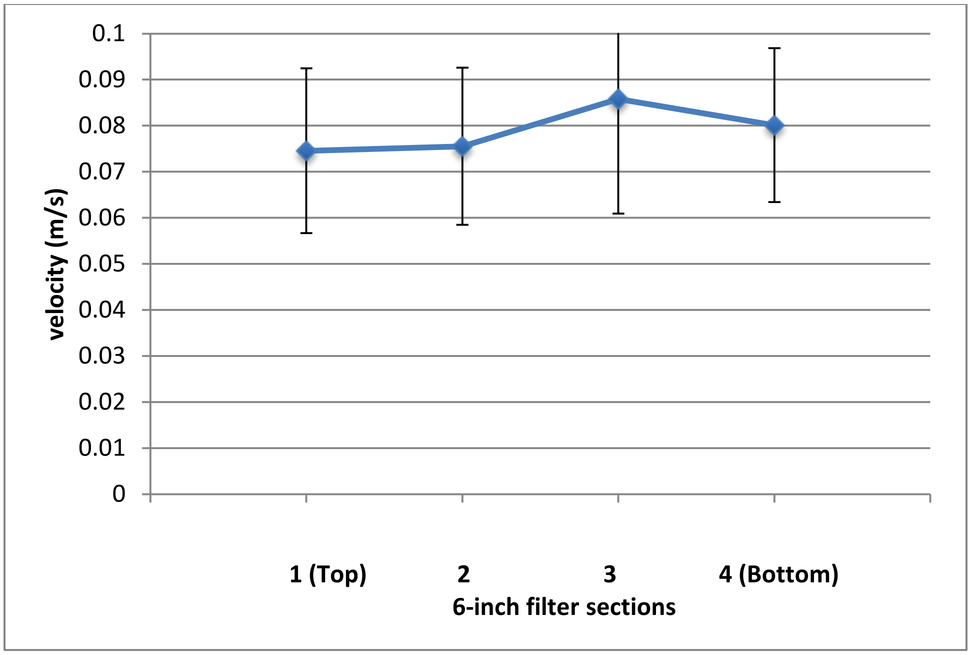

Figure 12: Velocity profile average values and standard deviation of UC <1.6 media

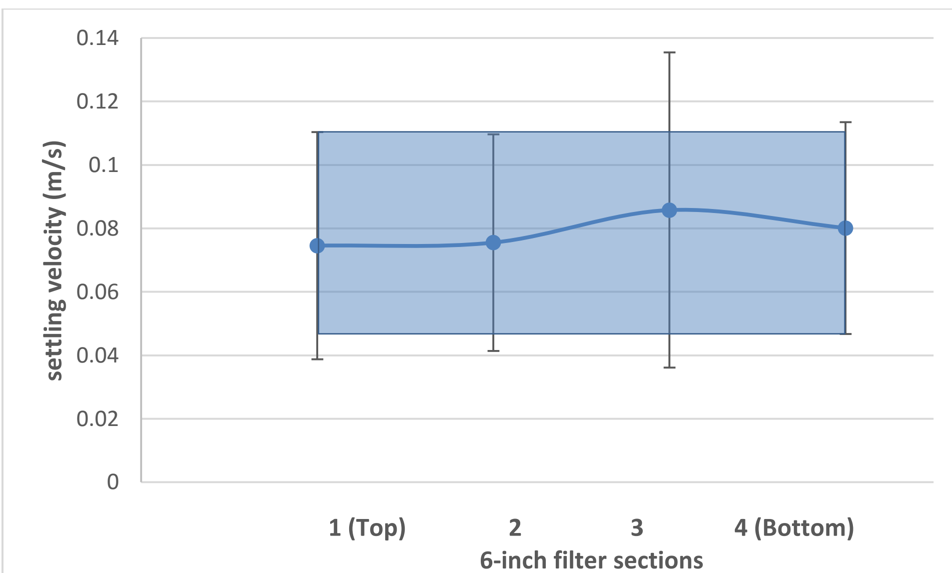

Figure 13: Stratification diagram with 95% confidence interval of UC <1.6 media

4.1.4 Four-Inch Column

A test was also carried out utilizing a larger 4-inch filter column with 24 inches of the <1.6 uniformity coefficient anthracite. The plan was to negate any possible wall effects or limitations of the smaller 2-inch filter column. As seen in Figure 14, stratification did not change significantly by increasing the size of the filter column. Results are very similar to previous tests using the 2-inch column and average settling values remain in the same range as the 2-inch column values. The 4-inch column also yielded the same large standard deviations from average values as previous tests.

The same stratification quantification method was again applied to the 4-inch column and results matched very closely to those of the 2-inch column for the same media with 89% of the media particles falling within the overlapped range of 0.049-0.098 m/s and 11% remaining stratified as is shown in Figure 15.

An ANOVA test did show a significant difference between all four populations with a P value of 0.003. Table 3 shows the t-Test results between all sections of the filter. A statistical significant difference is seen only between sections 1 and 3, and 1 and 4 indicating that there is some stratification occurring between the top and bottom of the filter.

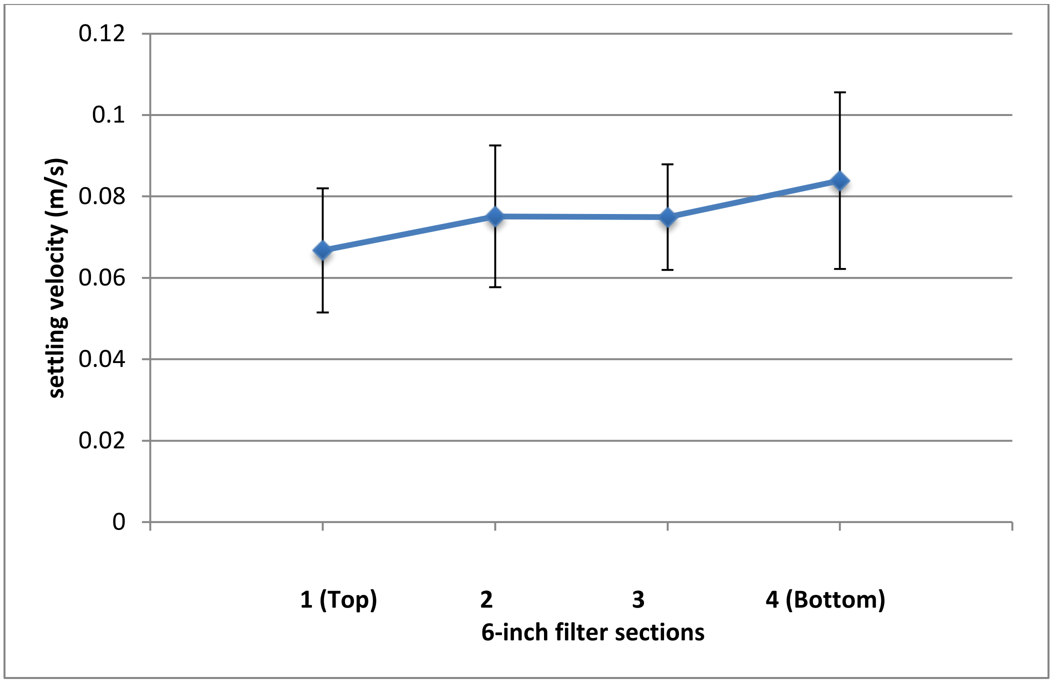

Figure 14: 4-Inch filter column velocity profile average values and standard deviation using UC <1.6 media

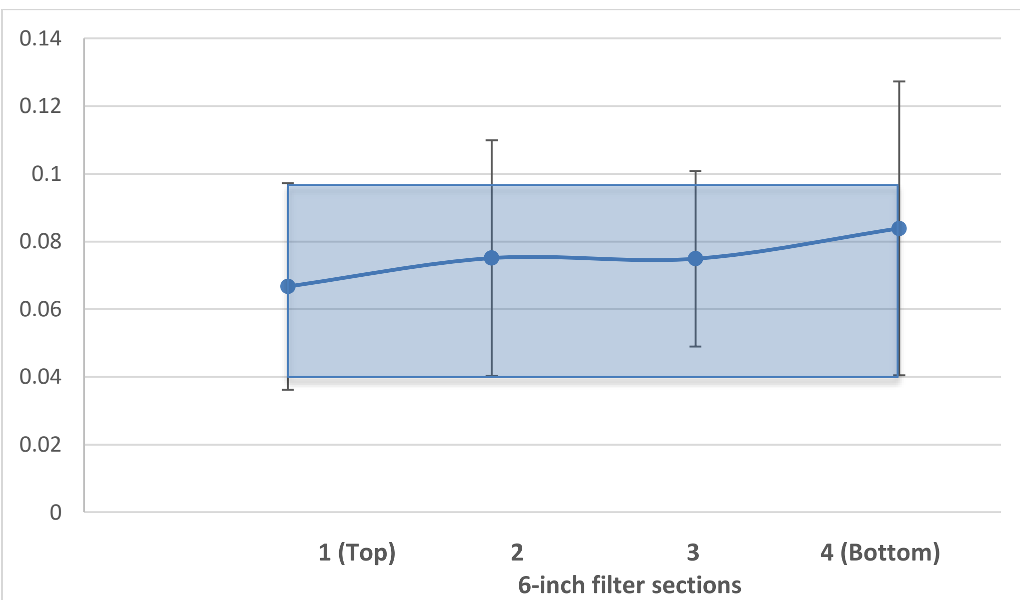

Figure 15: Stratification diagram with 95% confidence interval of UC <1.6 media in a 4-inch column

Table 2: t-Test results comparing settling velocity between 6-inch filter sections of the 4-inch column

Filter sections	**P value of 4-inch column anthracite sections**
1 and 2	0.052
1 and 3	0.029
1 and 4	<0.0001
2 and 3	0.96
2 and 4	0.090
3 and 4	0.058

4.1.5 Mt. Holly Core Sample Results

The Mt. Holly Water Treatment Plant uses dual media filters with a 10-inch Leopold block underdrain layered with 12 inches of support gravel with specific gravity of greater than 2.5 followed by 9 inches of sand with effective size 0.35-0.55 mm, a uniformity coefficient of <1.7, and a specific gravity of at least 2.5; 20 inches of anthracite with effective size of 1.0 mm, a uniformity coefficient of 1.3 and a specific gravity of 1.57 are layered above the sand. The total depth of anthracite, sand and gravel was 3.42 feet with a water depth of 8 feet and a max filtration rate of 3.82 gpm/sq ft.

Velocity profile results of the settling velocity test of the Mt. Holly core sample shown in Figure 16 matched pilot scale results almost identically (Figure 17). While it may seem that there is a slight upward trend in settling velocity from the top of the filter to the bottom, there is only approximately a 0.01 m/s difference in average settling velocity between the top and the bottom of the anthracite layer of the filter. This would indicate that stratification in conventional filters does not occur to the degree previously thought. Additionally, the now-familiar large standard deviations indicate that there is a lack of stratification between sections of the filter core sample profile in terms of settling velocity. These results also help to negate possible wall effects or skewed laboratory results based on pilot-scale setup. Statistical analysis showed a difference between all four populations with a P value of 0.0018, yet t-Tests between all adjacent filter sections were not found to be statistically different. Additionally, t-Tests between the same sections from Figure 16 and Figure 8 were all found to show no statistically significant difference with P values of 0.075, 0.15, 0.88 and 0.88 for sections 1, 2, 3, and 4 respectively. This indicates that the pilot-scale filter operates similarly to conventional filters.

Stratification was quantified in the same manner as pilot scale tests, and it was found that 85% of the media fell with the overlapping area of 0.053-0.088 m/s with 15% of the media remaining stratified (Figure 18). Table 3 shows the comparison of t-Test data.

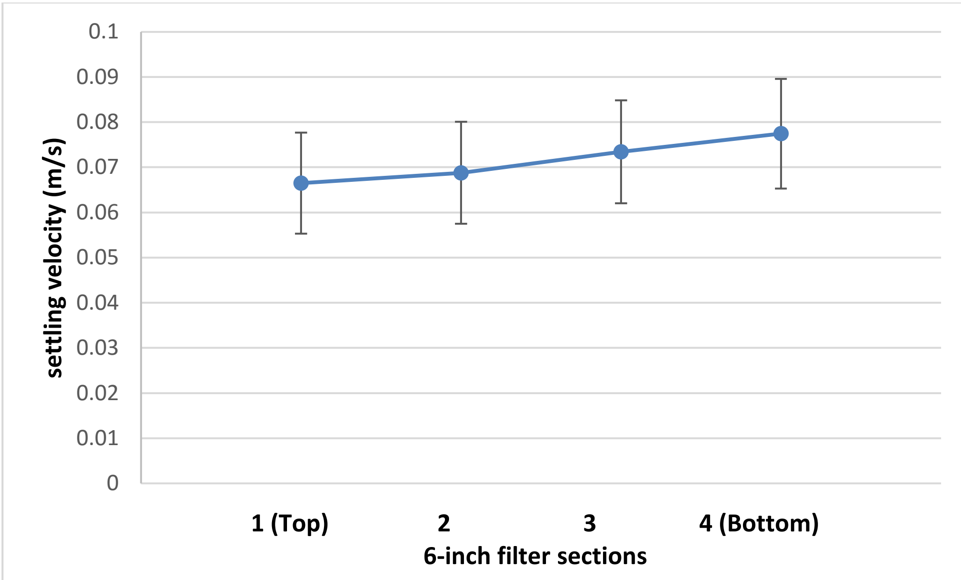

Figure 16: Velocity profile of Mt. Holly filter core sample settling test

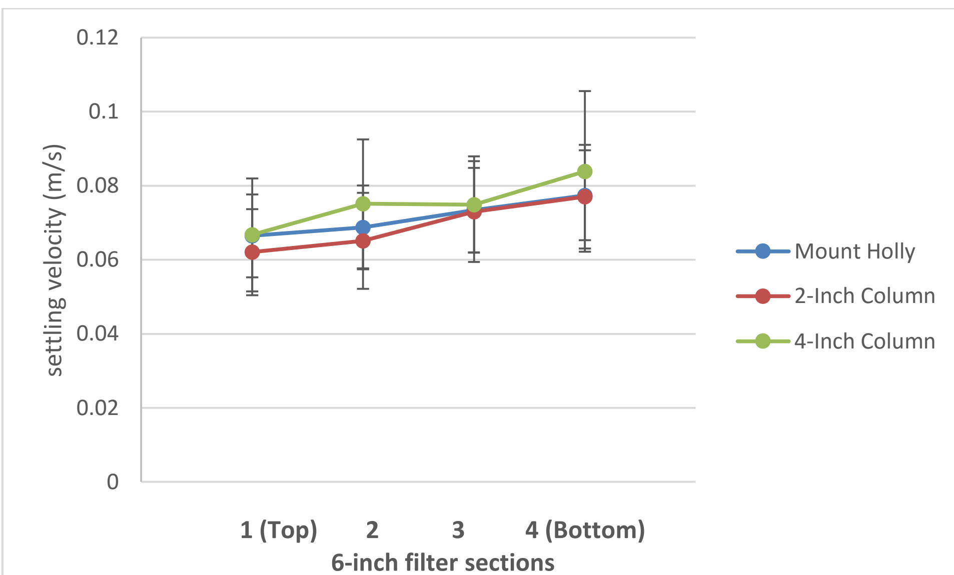

Figure 17: Comparison of full-scale, 2-inch and 4-inch column settling velocity profiles

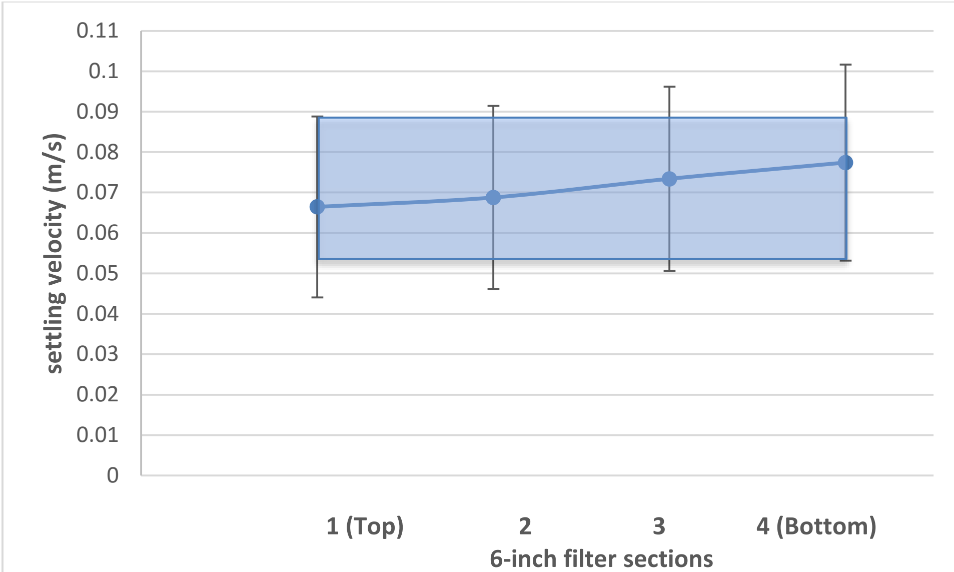

Figure 18: Stratification diagram with 95% confidence interval of Mt. Holly core sample

Table 3: Stratification Comparison between Mount Holly and 2-Inch Filter Column

	Mount Holly Core Sample Stratification	**2-Inch UC <1.5 Filter Column Stratification**
Overlapped settling velocity range	0.053-0.088 m/s	0.049-0.091 m/s
Percent overlapped	85%	87%
Percent stratified	15%	13%

4.1.6 Shape Analysis

Anthracite media particles, as mentioned in the methods section, were measured on a 3 dimension basis of length, width and height with length being the largest dimension and height representing the smallest dimension using a digital caliper. Each of these dimensions was analyzed individually relative to settling velocity in order to isolate significant variables.

4.1.6.1 Length (Largest Dimension)

From Figure 19, which highlights data from the triplicate settling velocity experiments, there is little correlation seen between the largest dimension of a particle and the settling velocity as is evident by the R^2 value of $3x10^{-4}$. Looking at Figure 20, particles of varying length dimensions are seen in all sections of the filter column and span a wide range of settling velocities. However, Figure 20 also shows that some stratification appears to be occurring as the fastest settling as well as the largest particles are mostly seen in the bottom 6 inches of the filter column indicating that other factors are contributing to settling velocity.

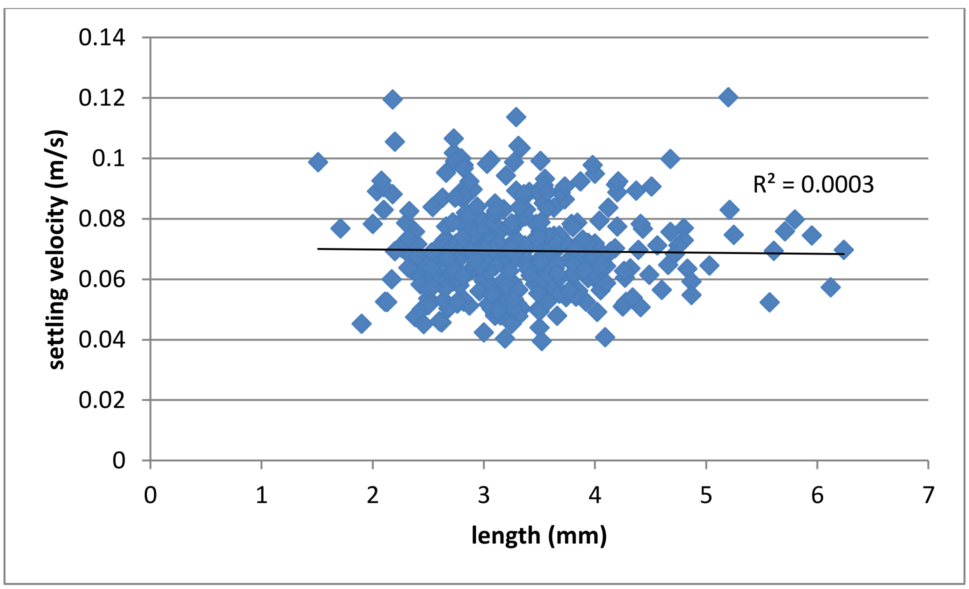

Figure 19: Combined UC <1.5 media tests of largest dimension versus settling velocity

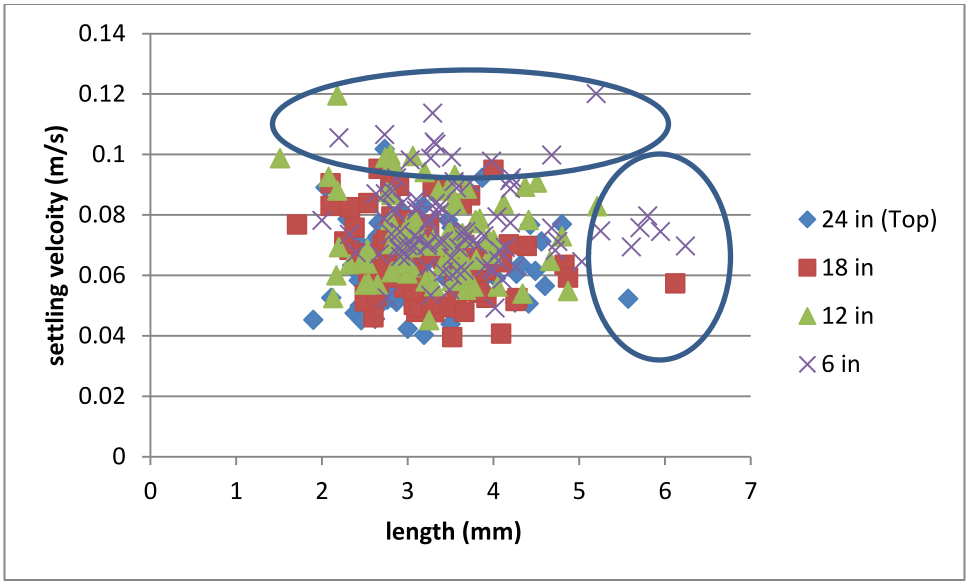

Figure 20: Combined UC <1.5 media tests of largest dimension versus settling velocity shown by section of the filter column showing stratification

4.1.6.2 Width (Middle Dimension)

Again in Figure 21, there is no correlation between width and settling velocity with the R^2 value of 0.025. Additionally, particles of a wide range of settling velocities appear in all sections of the filter. Results resemble those of Figures 19, and 20 indicating that this dimension is also not a good predictor of settling velocity.

Less stratification is seen with the middle dimension than the largest dimension, however it again appears that the fastest settling particles are found in the bottom 6 inches of the filter column as is shown in Figure 22.

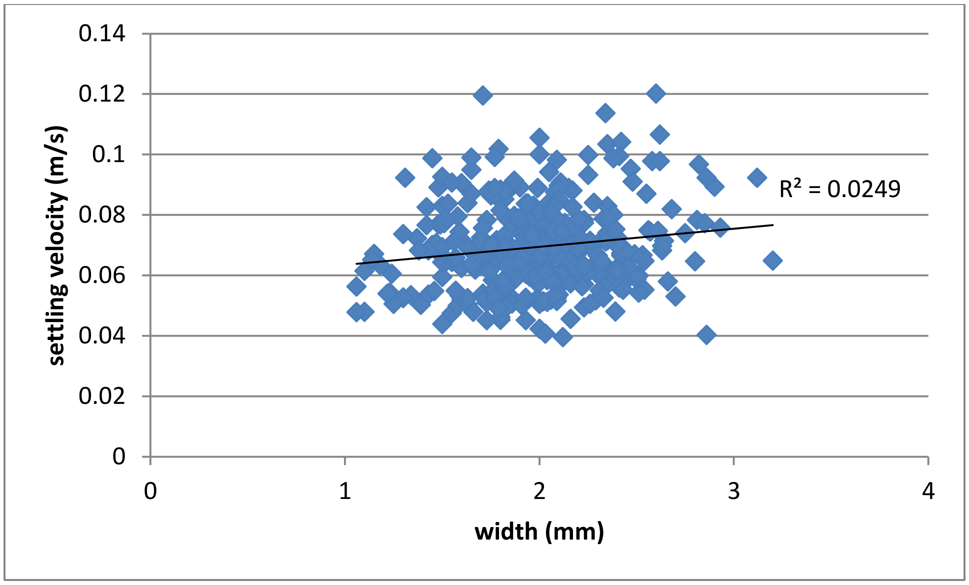

Figure 21: Combined UC <1.5 media tests of middle dimension versus settling velocity

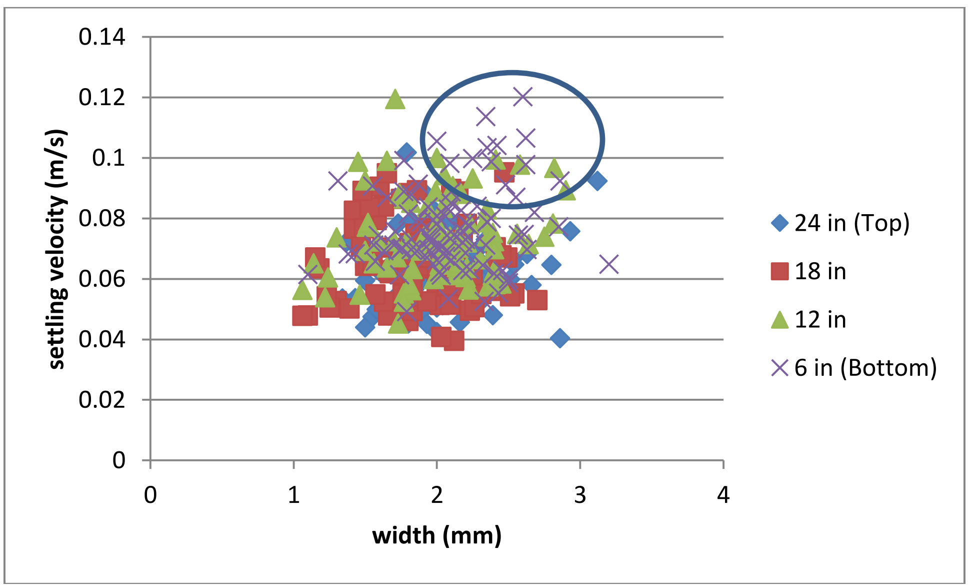

Figure 22: Combined UC <1.5 media tests of middle dimension versus settling velocity shown by section of the filter column showing stratification

4.1.7.3 Height (smallest dimension)

A more clear relationship between settling velocity and the smallest dimension emerges in Figure 23. A linear correlation between height and settling velocity is shown with an R^2 value of 0.50. This indicates that the smallest dimension is a possible predictor of settling velocity. Additionally, from Figure 24, one can see that these smallest dimensions are not isolated in sections of the filter but rather dispersed throughout the entire filter column. High and low settling velocities are seen in both the top and bottom sections of the filter indicating that there is not a distinct stratification occurring throughout the filter column in terms of settling velocity. However, it can also be seen in Figure 24 that the fastest settling particles are seen in the bottom 6-12 inches of the filter and the slowest settling particles are seen in the top 18-24 inches of the column indicating some level of stratification at opposite ends of the filter column.

This supports the theory that settling is controlled by shape as opposed to mass or size because height is independent of length and width with Figures 22 and 24 both showing a varied range of length and width dimensions for each section of the filter; indicating that size and mass are varied throughout the filter.

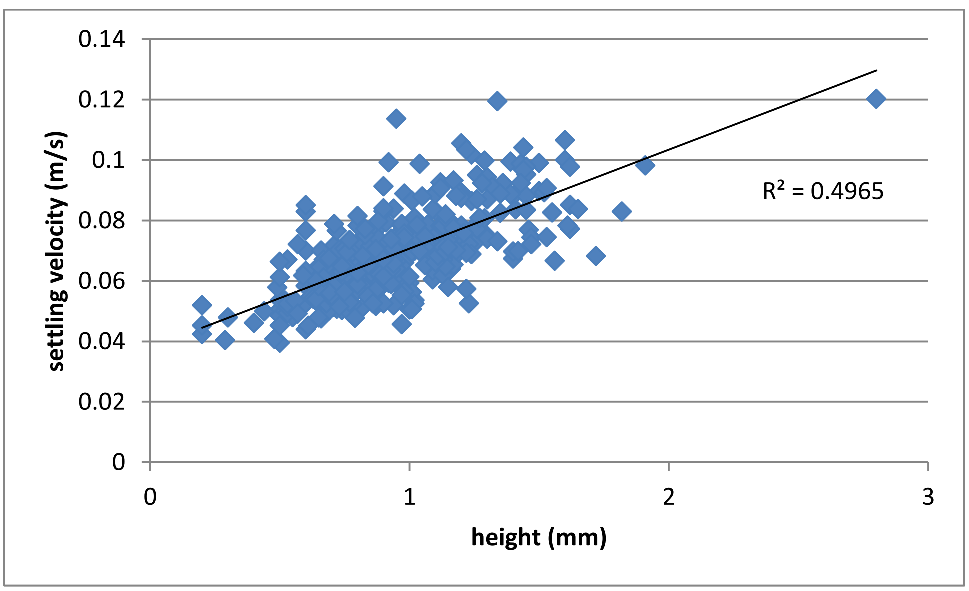

Figure 23: Combined UC <1.5 media tests of smallest dimension versus settling velocity

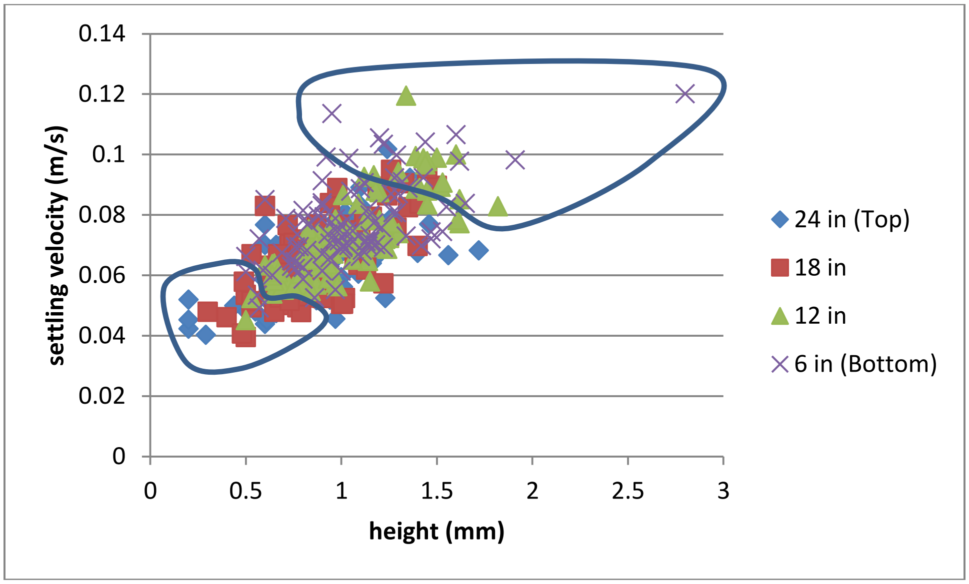

Figure 24: Combined UC <1.5 media tests of smallest dimension versus settling velocity shown by section of the filter column showing stratification

4.1.7.4 Smallest Dimension Profiles

To further analyze the results from Figure 24, Figure 25 shows how the height profile changes throughout the filter column from top to bottom. Overall, the average height seems to change little from top to bottom of the filter column ranging from about 0.85 mm to 1.05 mm. Additionally, there is a large standard deviation for each section of the filter column. This further indicates that the height is varying throughout each section of the filter. Because of this, the settling velocities throughout each section of the filter are varied as Figure 25 closely follows the velocity profile of Figure 8 as is seen in Figure 26. An ANOVA test on Figure 25 found significant difference between populations with a P value of $4.51\text{x}10^{-8}$. However, t-Tests of adjacent sections found no difference between the top 24 and 18 inch sections and bottom 6 and 12 inch sections with P values of 0.40 and 1, respectively. As was the case with data from Figure 8, a difference was found between the middle sections 2 and 3. This shows that height and settling velocity are correlated. Table 4 shows the t-Test results comparing height in all filter sections as well as settling velocity results for comparison.

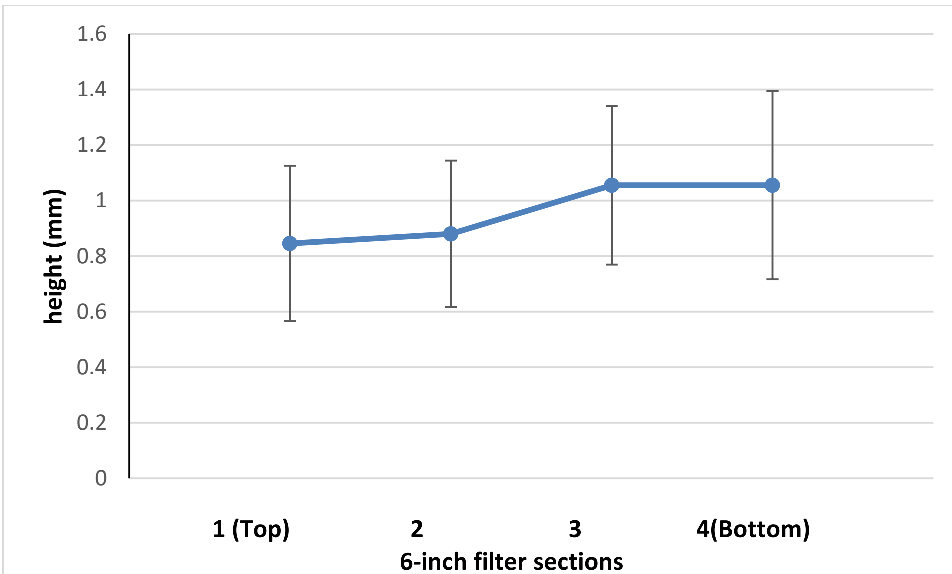

Figure 25: Combined UC <1.5 media smallest dimension profile average values and standard deviation from top to bottom of filter column

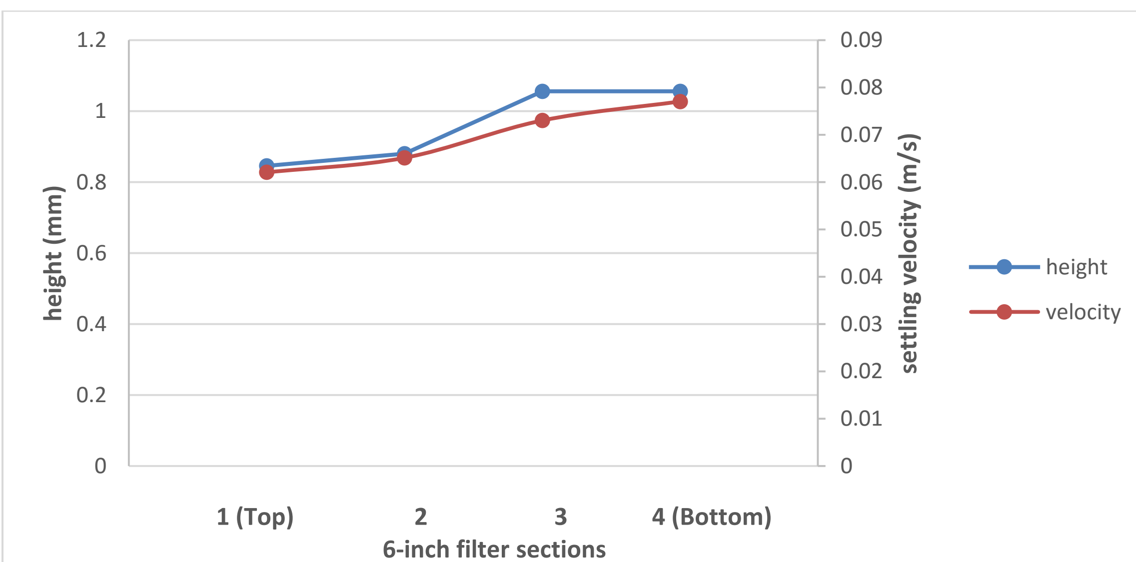

Figure 26: Comparison of height profile to settling velocity profile

Table 4: t-Test results of the smallest dimension (height) of anthracite through all sections of the filter compared with settling velocity P values from Table 1

Filter sections	**P values of smallest dimension of anthracite particles between filter sections**	**Settling Velocity P values of anthracite between filter sections**
1 and 2	0.40	0.099
1 and 3	<0.0001	<0.0001
1 and 4	<0.0001	<0.0001
2 and 3	<0.0001	0.0001
2 and 4	0.0002	<0.0001
3 and 4	1	0.052

4.1.7 Drag surface area

Calculated values for the drag surface area, the perimeter area of a falling particle parallel to the bottom of a settling column (as shown in Figure 27), reveal a linear correlation with an R^2 value of 0.35 (Figure 28). A level of error is to be assumed in calculations due to the irregularity of particle shapes. This indicates that drag surface area, along with height, may be a good predictor for settling velocity.

Figure 29 shows large standard deviations in drag surface area for each filter section. ANOVA test results of drag surface area found a significant difference between populations with a P value of 1.55×10^{-9}. T-Test results are found in Table 4. Results match those of the previous sections where the top two and bottom two adjacent sections do not show a difference, yet all other comparing sections show a statistically significant difference. Additionally, a correlation test found a strong correlation of 0.92 between the height and drag surface area profiles indicating that the two are related.

Drag surface area is more strongly impacted by a change in height since a change in height reflects a larger change in surface area than length or width as is seen in Figure 30 showing an R^2 value of 0.80 between height and drag surface area. However, there is a limitation on this analysis as drag coefficient and Reynold’s number which would affect the fluid displacement surrounding a falling particle as flow conditions changed were not considered for this study.

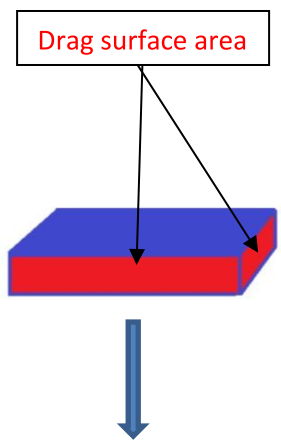

Figure 27: Drag surface area diagram

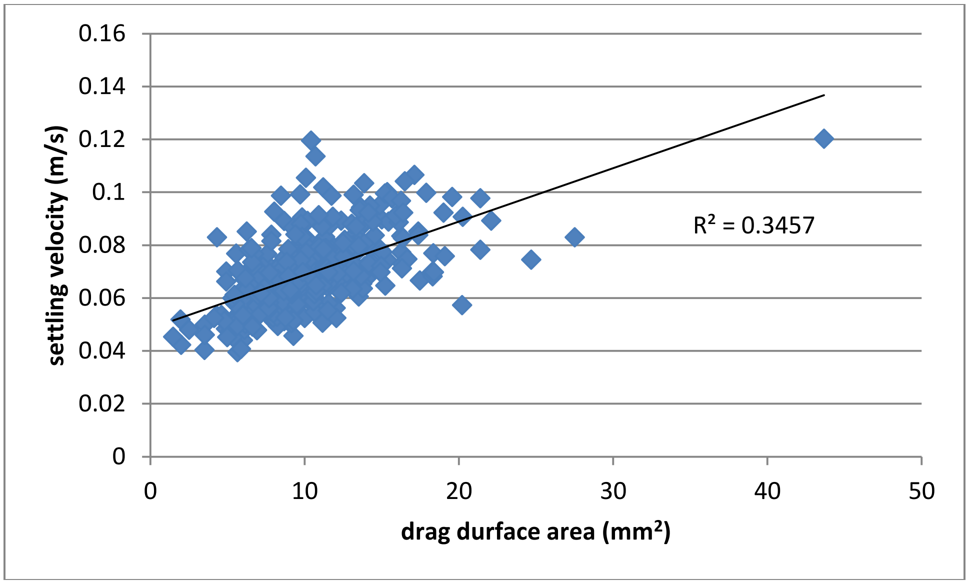

Figure 28: Drag surface area of UC <1.5 media

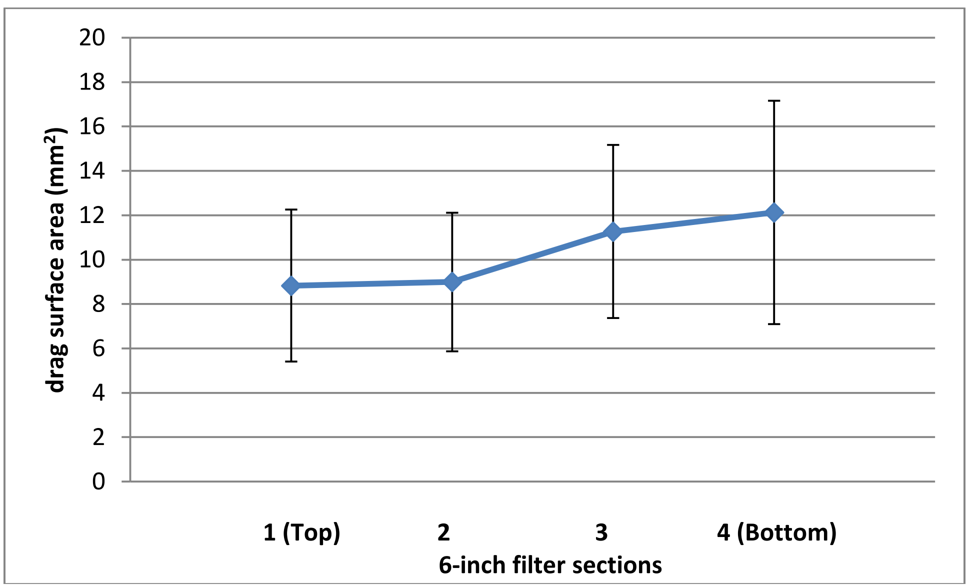

Figure 29: Drag surface area average values and standard deviation for UC <1.5 media

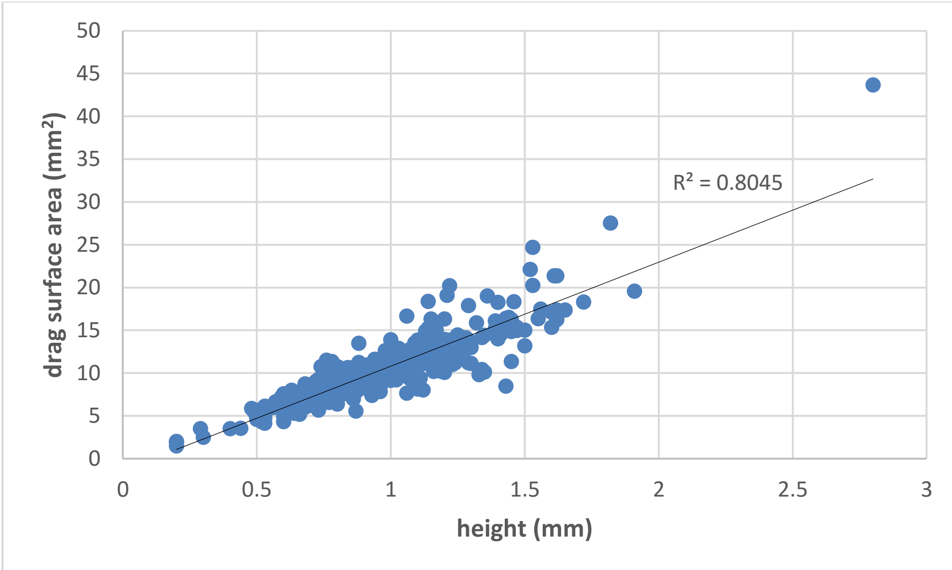

Figure 30: Comparison of height to drag surface area

Table 5: t-Test results of drag surface area

Filter sections	**P value comparing drag surface area between filter sections**
24” and 18”	0.74
24” and 12”	$1.71x10^{-5}$
24” and 6”	$8.76x10^{-7}$
18” and 12”	$2.87x10^{-5}$
18” and 6”	$1.48x10^{-6}$
12” and 6”	0.20

4.1.8 Anthracite Settling Velocity Model

Based on the dimensional analysis of height, and drag surface area, a model was developed to predict the settling velocity of the anthracite particles. Since the anthracite particles are irregular in shape, it was difficult to find a model that predicted the settling velocity of the anthracite exactly. Equation 18 incorporates the smallest dimension or height (mm), and the drag surface area (mm^2) which both showed correlations with settling velocity. When plotted against observed settling velocities for anthracite, the model produced an R^2 correlation of 0.44 as is seen in Figure 31.

$$\upsilon \left(\frac{m}{s}\right) = \frac{h^2}{A_{drag}} \qquad (18)$$

Table 6 shows the results of this model when used against 357 anthracite particles and their observed settling velocities. An average error of 36% was observed with median error of 29%. Although this model does not predict the settling velocity of every anthracite particle with complete accuracy, the model predicted the settling velocity with less than a 10% error for 20% of the anthracite particles, and less than a 30% error for 51% of the anthracite particles.

Table 6: Anthracite model results compared with observed settling velocities

Average Error	36%
Median Error	29%
Minimum Error	0.2%
Maximum Error	161%

<10% Error	20% of anthracite particles
<30% Error	51% of anthracite particles

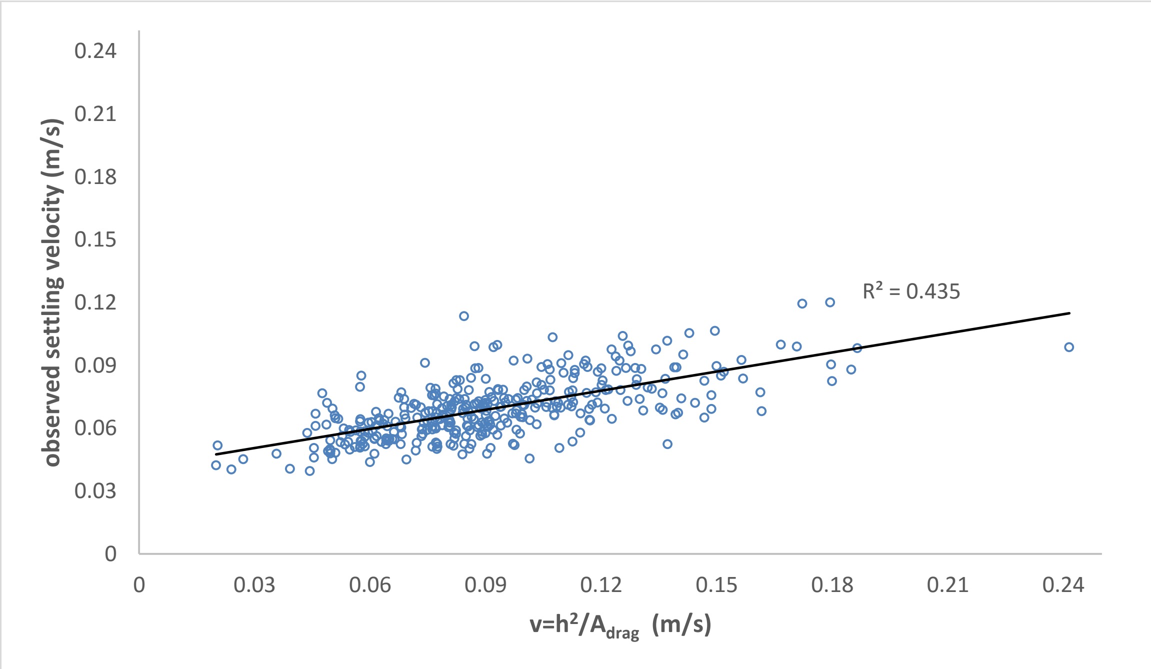

Figure 31: Anthracite model compared to observed settling velocity

4.2 Aluminum Analysis

The aluminum bars were cut in various lengths, widths and heights to form rectangular pieces. See Table 7 for sizes used. Dimensions were carefully chosen in a manner that would best assist in the isolation of a controlling dimension(s) in terms of predicting settling velocity. Initially it was thought there may be a correlation between all three dimensions and aluminum bars were cut with dimensions in ratios of one another (i.e. 4:2:1). A second set of aluminum bars were cut after analysis of the first set, which allowed for a deeper analysis of individual dimensions and the effects on settling velocity.

Table 7: Aluminum bar sizes tested

Length (in)	**Width (in)**	**Height (in)**	**Ratio**
1	0.5	0.125	8:4:1
0.5	0.5	0.125	4:4:1
0.5	0.25	0.125	4:2:1
1	0.25	0.25	4:1:1
0.5	0.25	0.25	2:1:1
0.25	0.25	0.25	1:1:1
0.38	0.38	0.09	4.2:4.2:1
1	0.38	0.09	11.1:4.2:1
0.75	0.38	0.09	8.3:4.2:1
1	0.5	0.19	5.3:2.6:1
0.75	0.5	0.19	3.9:2.6:1
0.5	0.5	0.19	2.6:2.6:1
1.5	0.38	0.38	3.9:1:1

Aluminum bars were analyzed to better understand and determine how each dimension affected settling velocity without the influence of irregular shape. Based on the results from the filter media columns, it was theorized that the smallest dimension played a significant role in the determination of settling velocity. However, there was little information to be determined from the length and width analyses. By carefully choosing various dimensions for length, width and height, these dimensions were able to be isolated and better understood as to how they affected settling velocity.

4.2.1 Settling Velocity

It should be noted that all aluminum bars tested oriented in the settling column with the smallest dimension falling parallel to the bottom of the settling column (Figure 32). Additionally, Reynold’s numbers were not considered during this study which presents a limitation on the analysis regarding dimensional effects and drag since calculated Reynold’s numbers for aluminum fell within the turbulent flow regime, while anthracite Reynold’s numbers indicated laminar flow. Table 8 shows the comparison of Reynold’s numbers between anthracite and aluminum.

Table 8: Reynold's number comparison between anthracite and aluminum

	Reynold’s number range	**Average Reynold’s number**	**Flow**
Anthracite	86-720	246	Laminar
Aluminum	4,360-15,933	8300	Turbulent

Figure 33 shows the settling velocity for all 100 aluminum pieces tested from the first set of aluminum bars. There are two clearly defined settling velocity range areas seen. This divide happens to correlate with the bars with a height of 1/8” being in the lower section and a height of 1/4” seen in the top section.

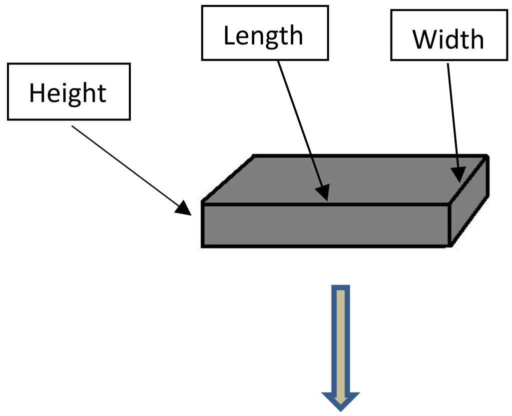

Figure 32: Aluminum bar settling orientation

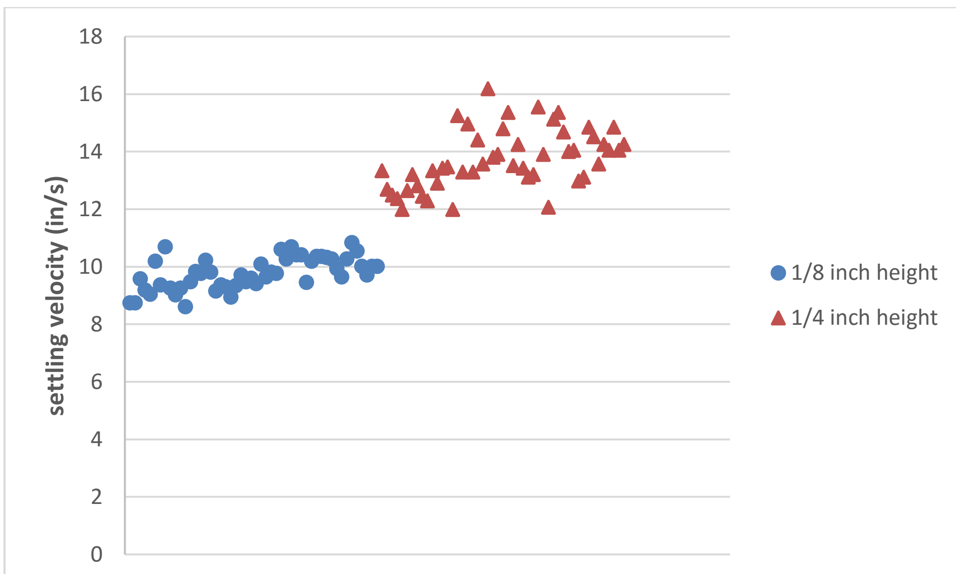

Figure 33: Settling velocity of aluminum bars from Set 1

4.2.1.1 Shape Analysis

Figure 33 shows a clear divide based on height, yet there is still a range of values within each of these two sections. The aluminum pieces with a height of 1/8" show a tighter velocity range while the pieces with a 1/4" height show a slightly wider range of settling velocities indicating that there are other factors affecting the settling velocity.

Figure 34 shows that as length increases, settling velocity changes little. The 1/4” length pieces show a wider range of settling velocity. For example, for the aluminum bars with a 1:1:1 ratio with all dimensions equal to 1/4”, there was a wide range of settling velocities as these aluminum pieces tumbled and rotated greatly as they settled. With all dimensions being equal, length, width and height are all fighting to be the controlling dimension. In addition, the 1/4” to 1/2” and 1/2” to 1” changes in length would suggest a doubling in mass for a given height, however this does not seem to affect the settling velocity based on Figures 34 and 35 indicating that length is not a controlling factor for settling velocity. This is consistent with the anthracite data in Figure 19 where there is no correlation seen between length and settling velocity.

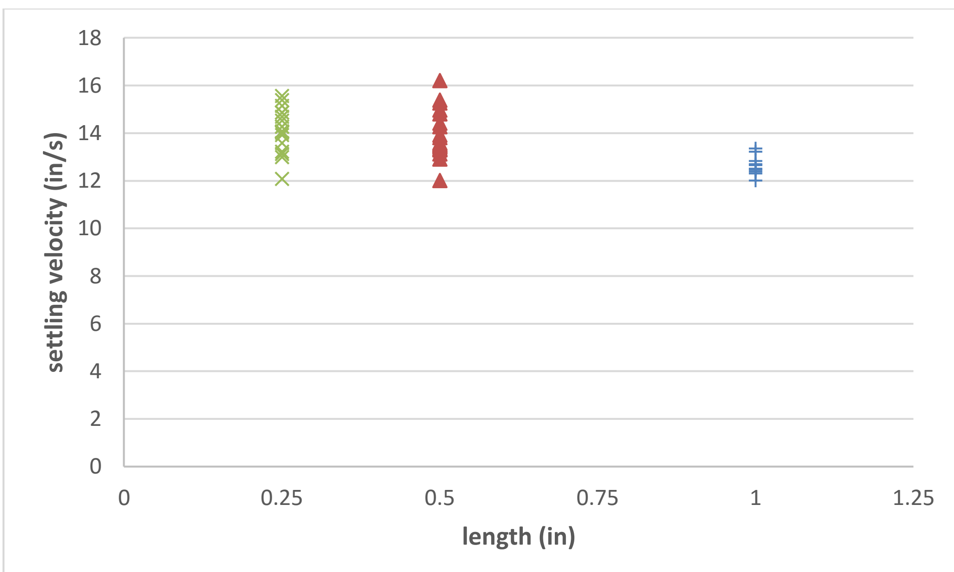

Figure 34: Comparison of length to settling velocity for aluminum bars with a height of 1/4 inch

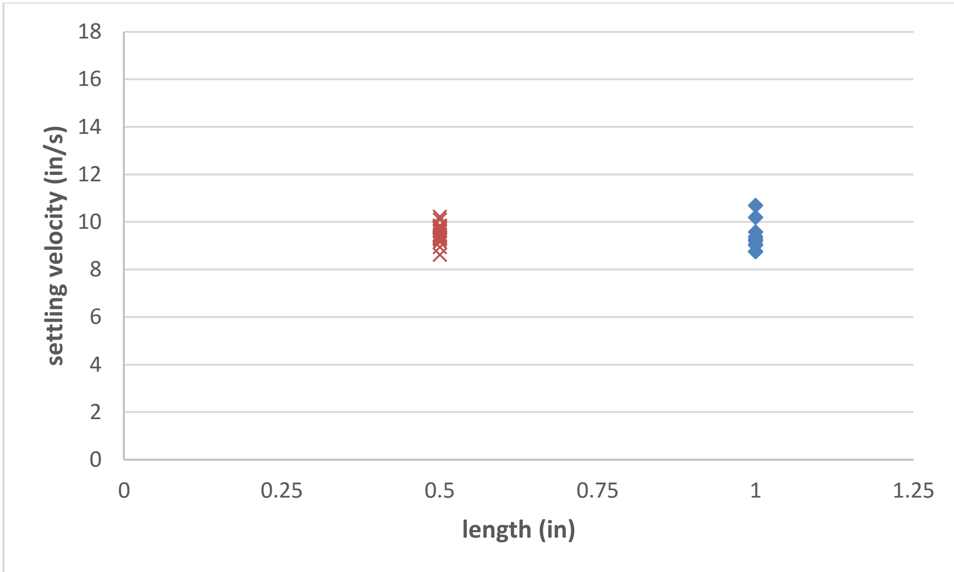

Figure 35: Comparison of length to settling velocity for aluminum bars with a height of 1/8 inch

Figure 36, representing the width, shows similar results to Figures 34 and 35 with the settling velocities from 1/4” overlapping the settling velocity of 1/2” pieces, however the 1/4” width pieces have a wider range of settling velocities.

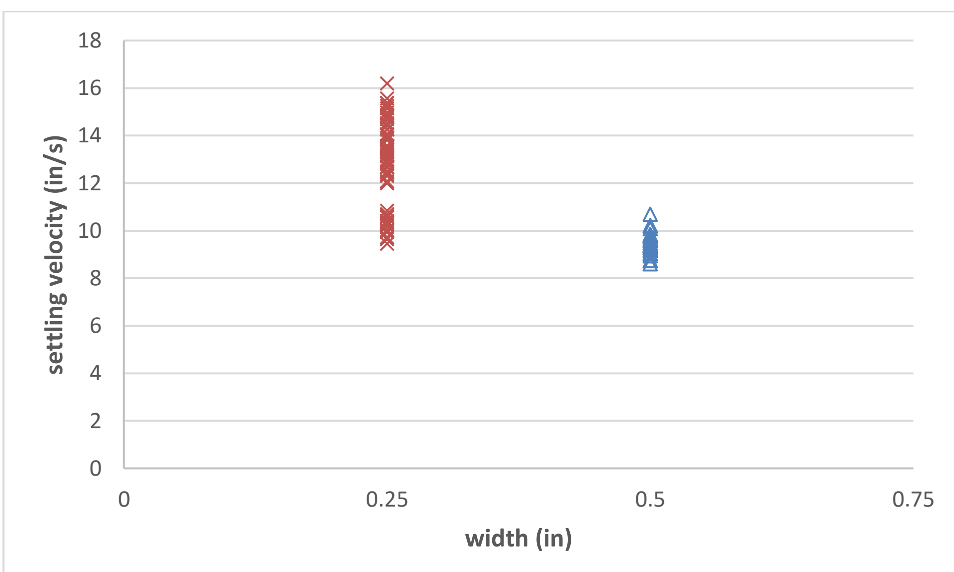

Figure 36: Width of aluminum bars versus velocity from Set 1

However, in looking at Figure 37, there is a clear distinction between height dimensions of 1/8" and 1/4". Once again, this strengthens the theory that height is a controlling dimension for predicting settling velocity.

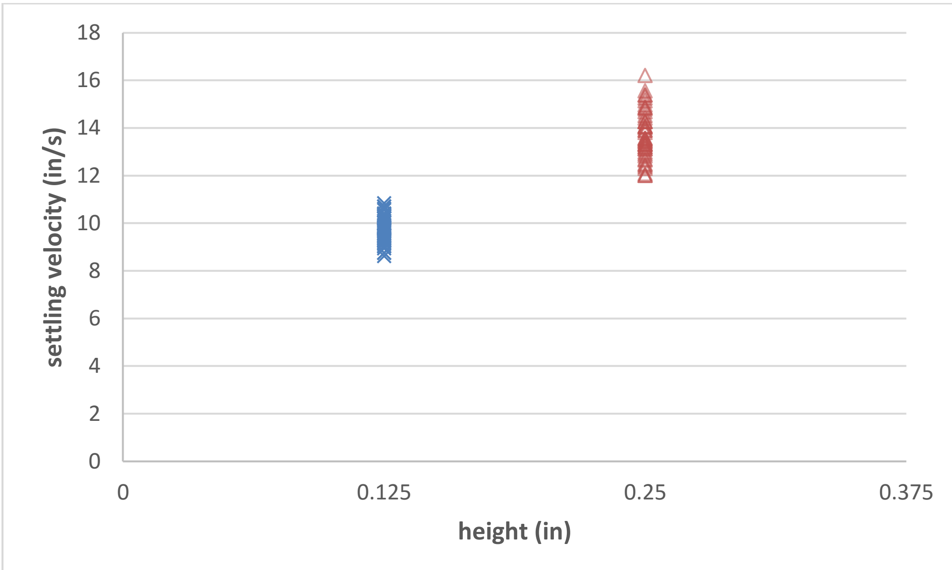

Figure 37: Height of aluminum bars versus velocity from Set 1

In Figure 38, the particles of differing drag surface areas but of the same height dimension had similar settling velocity ranges, which further indicates that height is a controlling dimension. Additionally, a t-Test showed a statistically significant difference between the drag surface area of the 1/4 inch height bars and the 1/8 inch height bars with a P value of <0.0001. While overall, drag surface area showed a wide range of settling velocities, the range for aluminum bars with a drag surface area of ¼ in^2 and 3/8 in^2 was relatively the same, and the settling velocities for the aluminum bars with drag surface areas of 3/16 in^2 and 5/8 in^2 fell within that range indicating that drag surface area is only a controlling factor when compared to height.

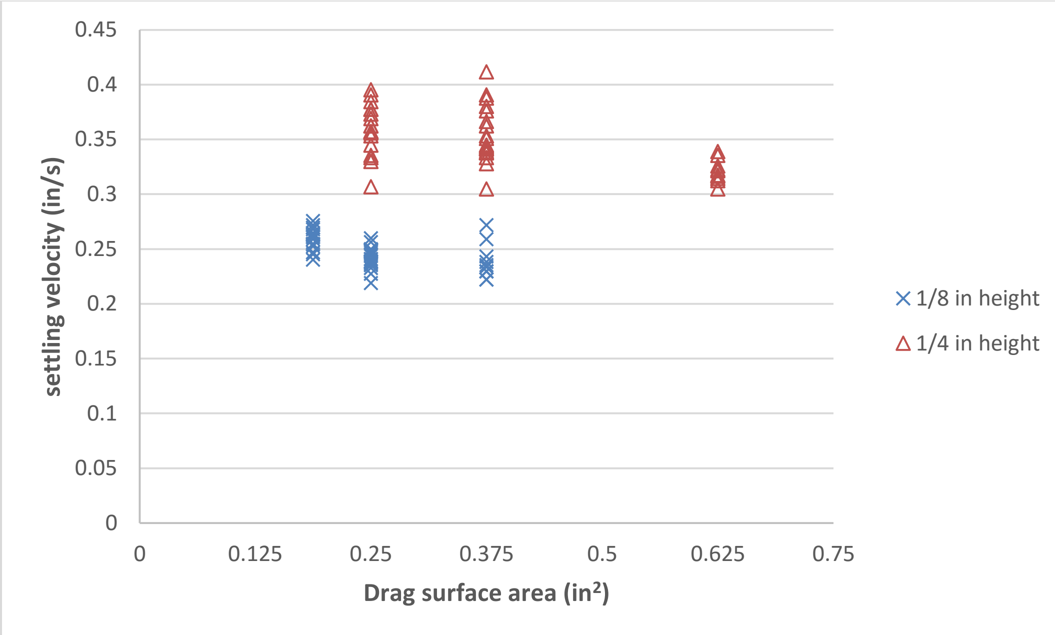

Figure 38: Surface area of aluminum particles versus velocity

4.2.2 Second Aluminum Set

Following the analysis of the first set of aluminum bars, another set of aluminum bars were tested to further analyze the effects of length, width and height independent of particle ratio (Table 7). Results of these tests closely mirrored those of the first set. Therefore data from set 1 and 2 were combined to show overall results.

4.2.2.1 Settling Velocity

Figure 39 shows the settling velocity results from all 175 aluminum pieces tests from Sets 1 and 2. The figure shows the clear grouping of settling velocities by the smallest dimension. Although the settling velocity within each height dimension does vary some, it is evident that the smallest dimension is controlling these settling velocities as there is a linear trend seen as the smallest dimension increases. Figure 40 also shows that the change in height reflects a strong linear correlation with an R^2 value of 0.90.

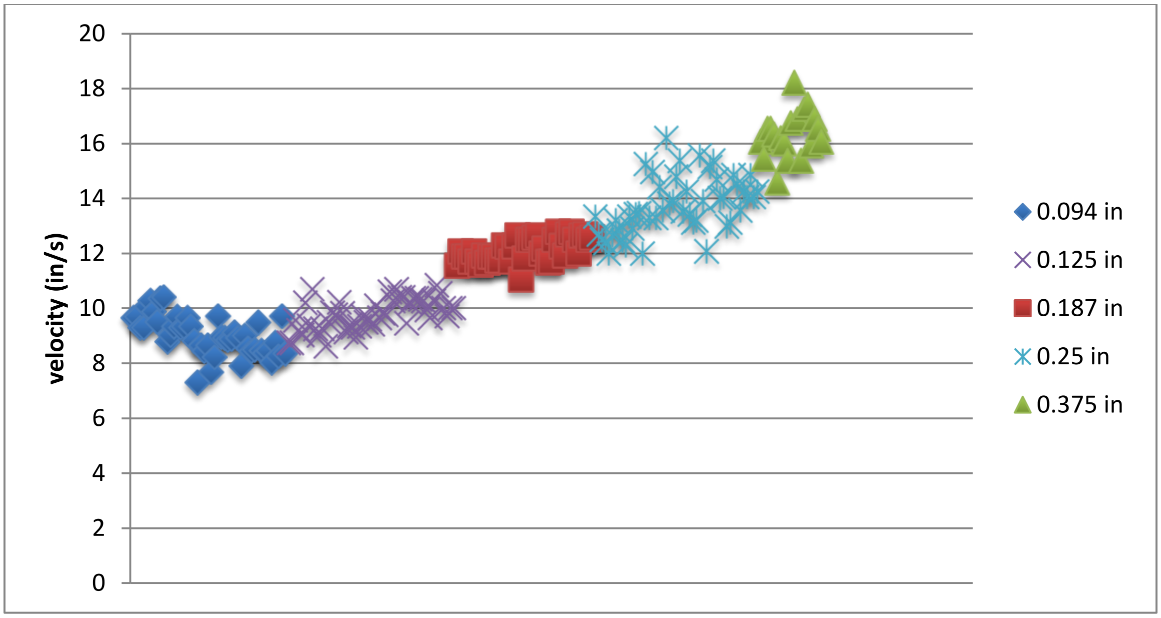

Figure 39: Velocity of all aluminum bars tested stratified by height

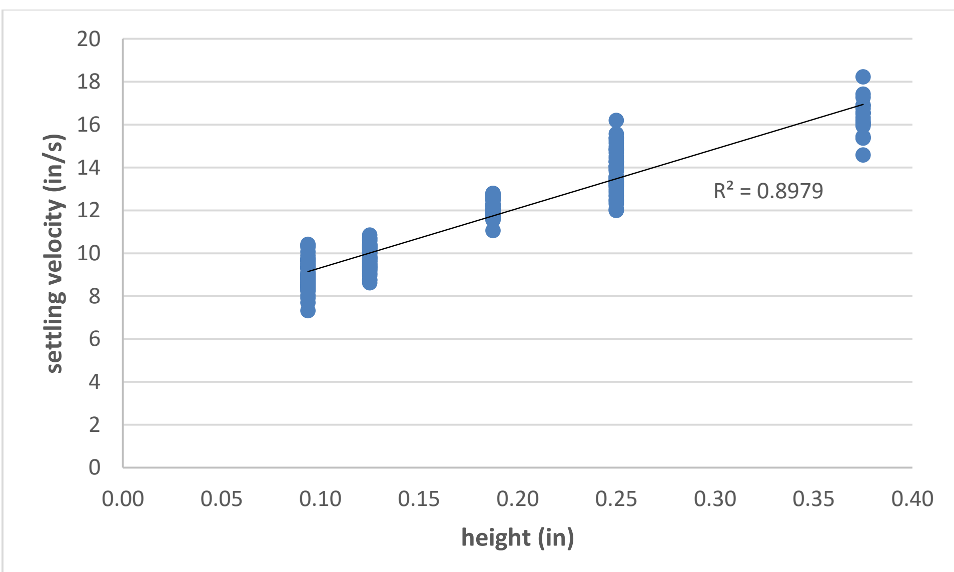

Figure 40: Height versus settling velocity linear correlation

Figure 41 shows the mean values and standard deviations from these aluminum bars displaying that these dimensions hold consistent in their effect on settling velocity. Other effects such as drag and surface area will be further analyzed.

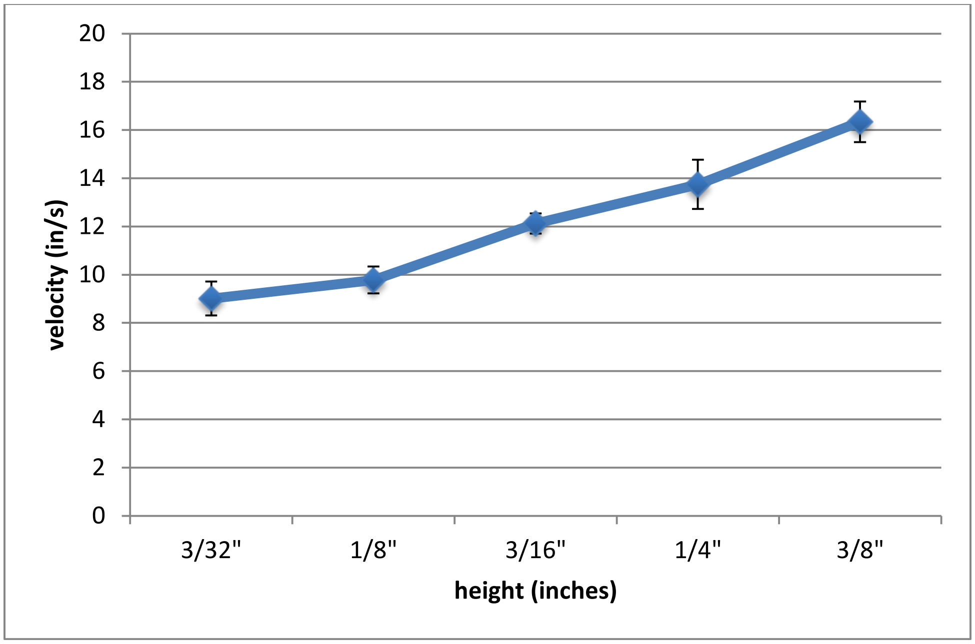

Figure 41: Average values and standard deviations from aluminum bars grouped by height

4.2.3 Empirical Equations

Three empirical equations (Equations 19, 20, and 21) were developed from the first set of aluminum bars where L is length (in), h is height (in), A_s is drag surface area (in^2), w is width (w), and υ is settling velocity (in/s). All three of the equations followed a similar format of two variables added in the numerator and then multiplied together in the denominator. The equations were developed with the intent of capturing the controlling variables of the settling velocity. Equations 19 and 20 showed to be the best predictors of settling velocity with average errors of 9.67% and 9.45% respectively, while Equation 21 had an average 13.94% error over all pieces from the first set. Pieces with a height of 1/8” had a lower percent error averaging 4.54%, 4.39% and 10.49%, respectively for Equations 19, 20, and 21. Larger error was seen with a height of 1/4”. All three equations contain the smallest dimension while relating it to the other dimensions and variables.

From the results of the equations, it would seem that length and surface area are recurring in terms of settling velocity prediction.

$$\nu = \frac{L+h}{L*h} \qquad (19)$$

$$\nu = \frac{h+As}{h*As} \qquad (20)$$

$$\nu = \frac{h+w}{h*w} \qquad (21)$$

4.2.4 Three-Dimensional Graphs

Following the development of the empirical equations and analysis of the aluminum particles, it became evident that height was a controlling dimension, however it was not possible to single out the other variables without further analysis. Three-dimensional plots proved necessary to truly analyze the varying effects the shape and dimension orientation had on settling velocity.

4.2.4.1 Height and Width

Figure 42 comparing height and width to settling velocity shows an increasing trend as height increases for a particular width. It is difficult to analyze the effect of width since there are only two comparable data points. However the graph would suggest that width is not a strong predictor of settling velocity as compared with height based on the observation that for a height of 1/8”, there is little difference in settling velocity between a width of 1/4”and a width of 1/2”.

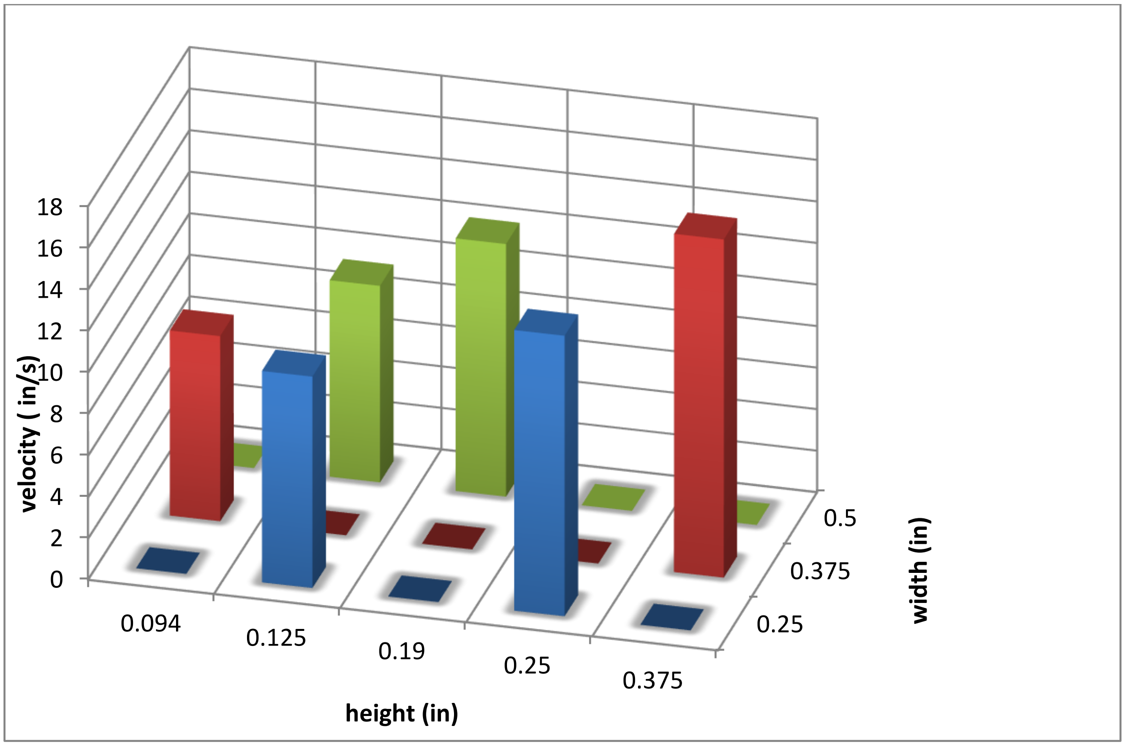

Figure 42: Three-dimensional graph comparing height and width to settling velocity

4.2.4.2 Height and Length

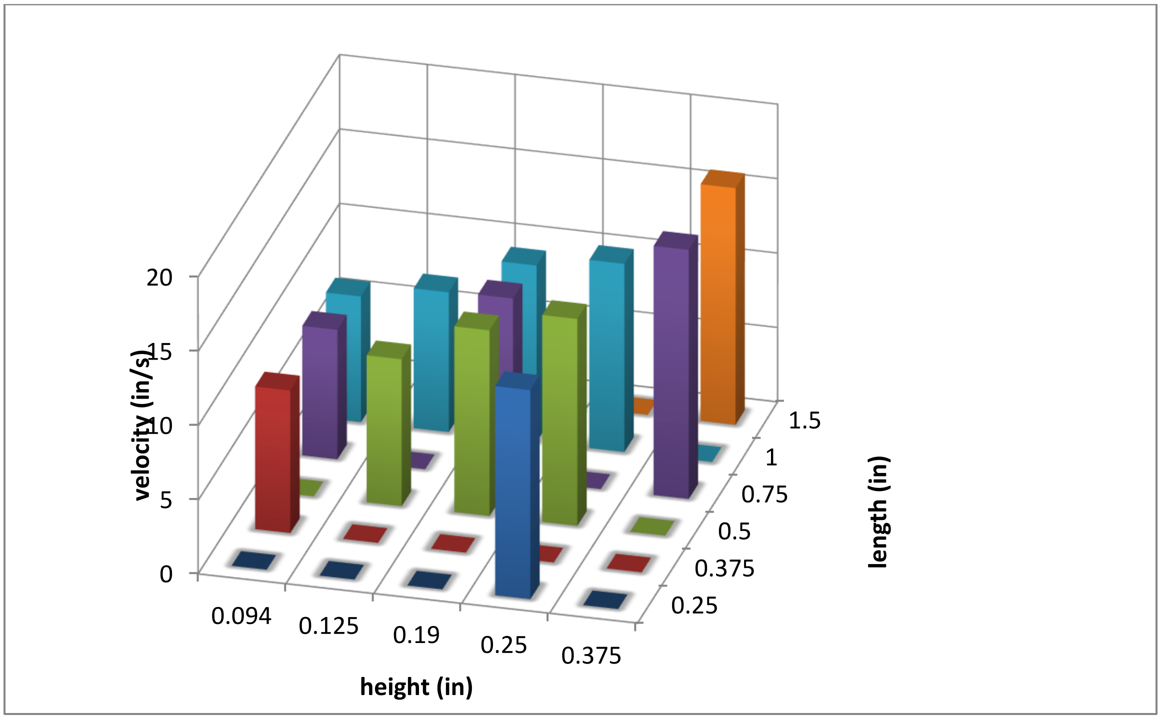

Figure 43: Three-dimensional graph comparing height and length to settling velocity

Figure 43 shows that, the smallest dimension shows an upward trend in the settling velocity as the dimension is increased as compared to the largest dimension. In the graph, it can be seen that as length increases for a particular height, the settling velocity remains relatively unchanged. However, for a particular length, settling increases almost uniformly across all height dimensions shown. Because of this trend, length is shown to have little importance of the prediction of settling velocity and places an increasing importance on the smallest dimension as a controlling variable.

4.2.4.3 Height and Drag Surface Area

Figure 44 is the first plot that begins to show a relationship between two variables for control over settling velocity. It can be seen that as height increases so too does the settling velocity, however this is not visibly the case with drag surface area. As previously defined, the drag surface area is the perimeter surface area of the particle falling parallel to the settling column bottom.

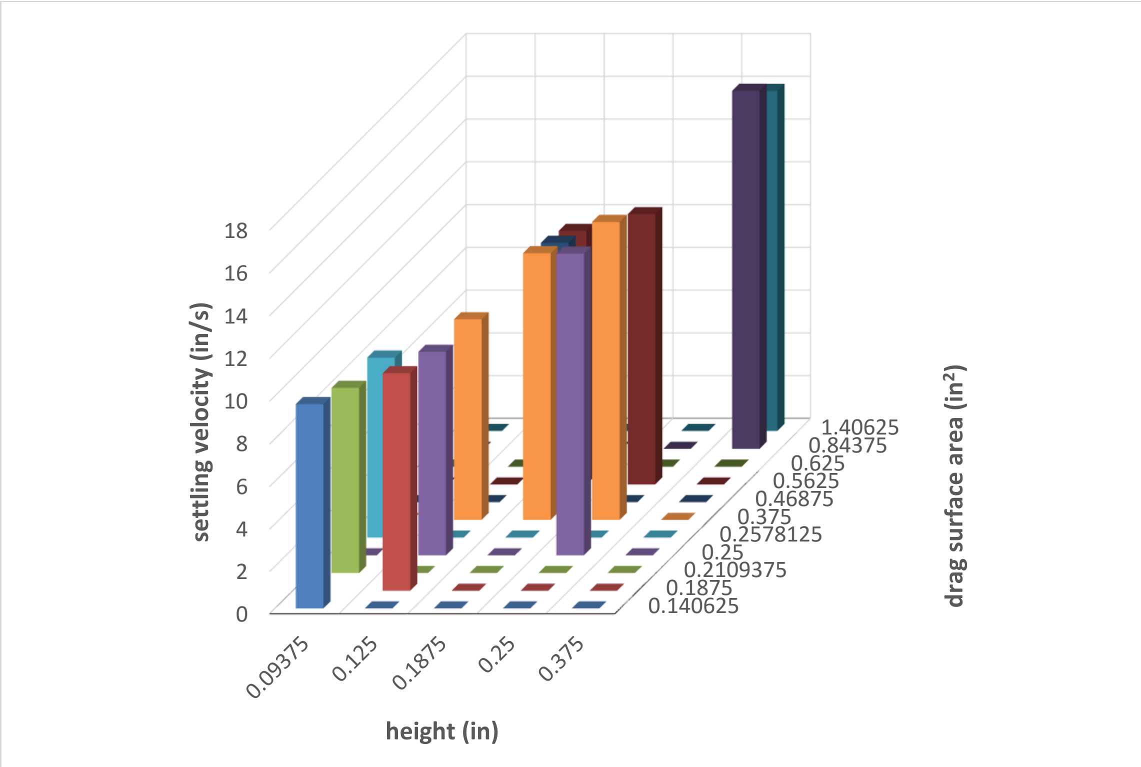

Figure 44: Three-dimensional plot comparing height and drag surface area with settling velocity

4.2.4.4 Mass and Height

There were many gaps in the dataset for Figure 45 as many of the particles coincidentally had the same mass despite having different dimensional makeups. Yet, results indicated that there was not a correlation between height and mass, which was not expected. Although settling velocity appears to increase as height increases, there is not a clearly defined trend as mass increases for a particular height. This would indicate that mass is not a reliable indicator of settling velocity and puts a stronger emphasis on other variables as a controlling factors in the prediction of settling velocity.

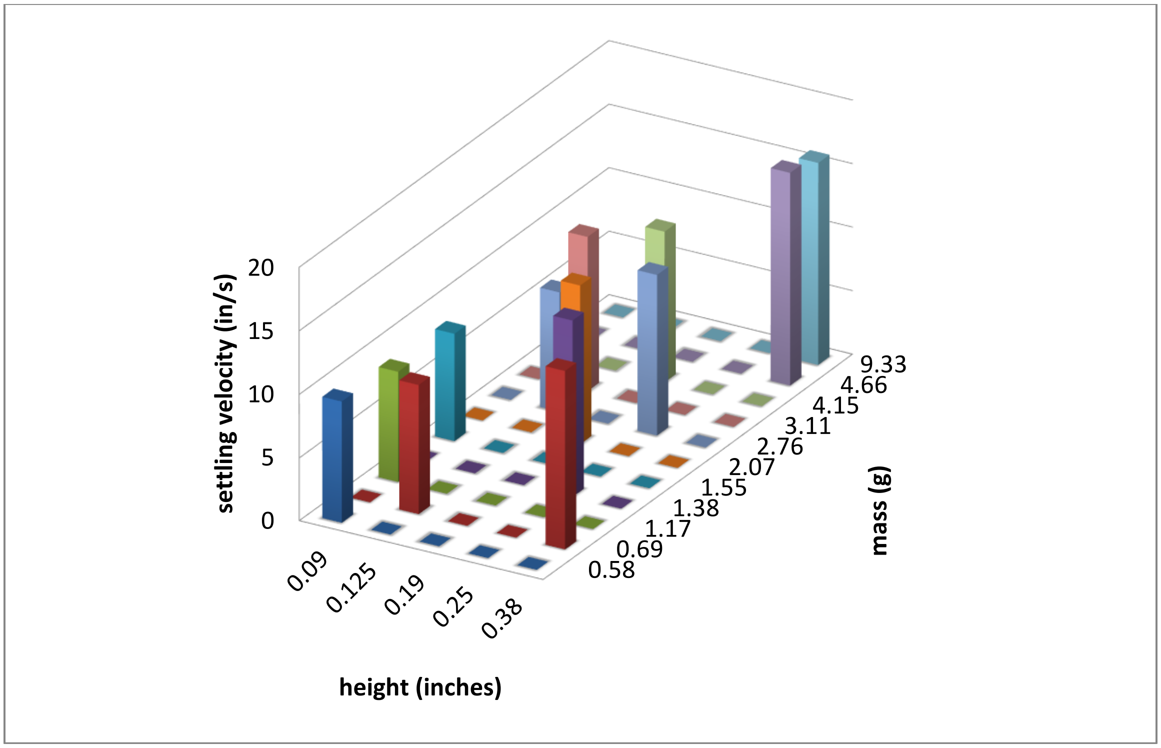

Figure 45: Three-dimensional plot of height and mass against settling velocity

4.2.4.5 Identifying Commonality

As noted previously, many of the graphs have gaps in the dataset, which proved difficult to analyze. In order to further investigate the controlling variables, data points were normalized by mass to rule out any variation that came with too many changing variables (Figures 46, 47, 48). There were three data sets that had at least two particles with identical masses. These particles were plotted against settling velocity with height and drag surface area as these appeared to be the two strongest indicators of settling velocity prediction based on Figures 38 and 40.

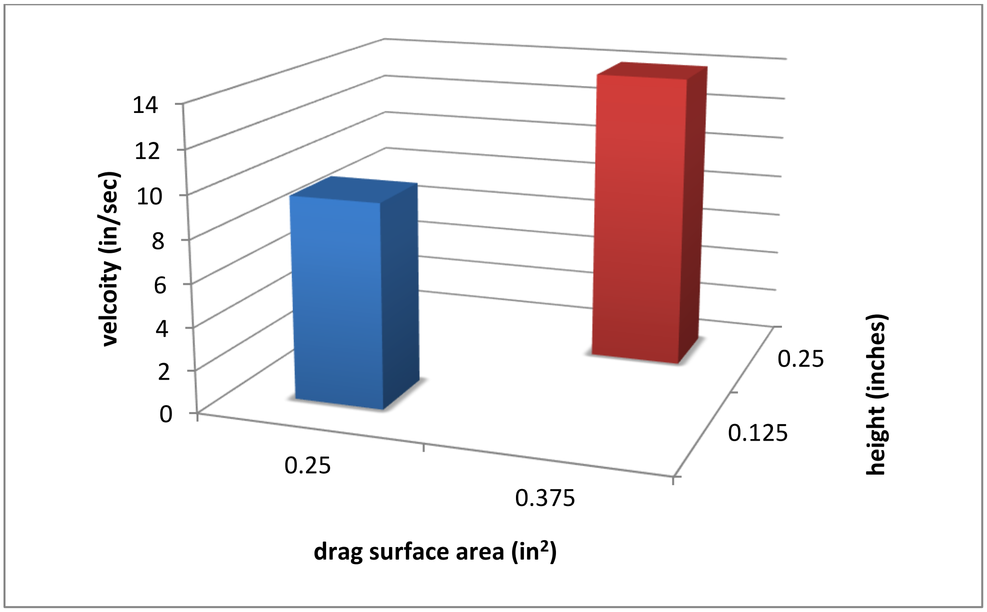

Figure 46: Plot 1; Three-dimensional graph of drag surface area and height against settling velocity for aluminum particles with mass= 1.38 g

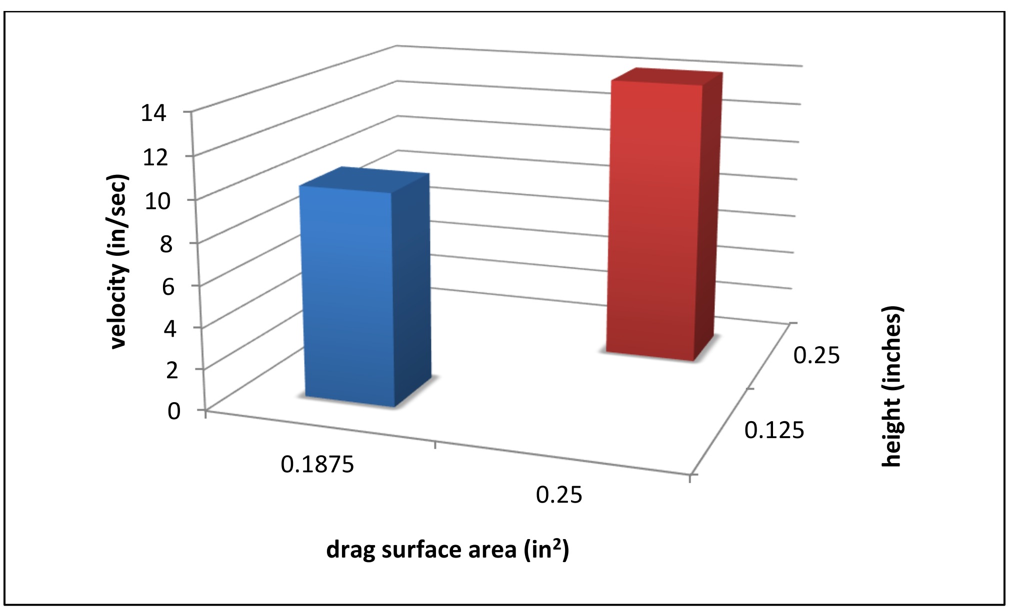

Figure 47: Plot 2; Three-dimensional graph of drag surface area and height against settling velocity for aluminum particles with mass= 0.69 g

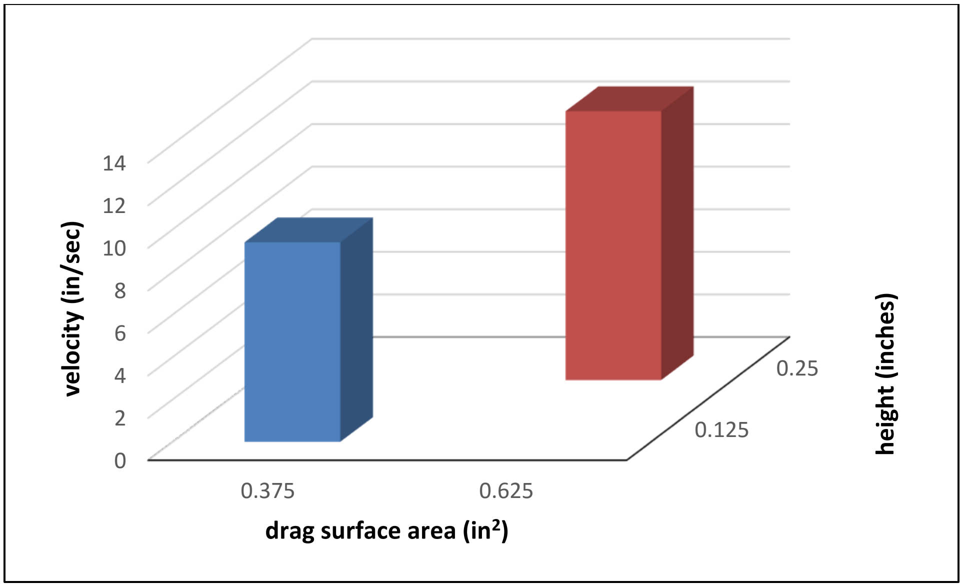

Figure 48: Plot 3; Three-dimensional graph of drag surface area and height against settling velocity for aluminum particles with mass= 2.76 g

4.2.4.6 Custom Pieces to Predict Settling Velocity

Furthering the analysis of Figures 46, 47, and 48, prediction of settling velocity based on the variables of height and drag surface area was attempted by finding a linear relationship between the variables. Vector notation was used to find dimensions that would produce a settling velocity that would fall linearly between the data points in each figure. Since length and width were not considered as important factors at this point in settling velocity prediction, dimensions were created to fit the median drag surface area and height for Figures 46, 47 and 48 (i.e. surface area and height were held constant to find length and width dimensions that would fit). Table 9 lists the developed pieces to be tested against each plot. Figures 46 (Plot 1) and 47 (Plot 2) both had two different aluminum bar pieces that fit the dimensional requirements.

Table 9: Custom aluminum pieces to fit normalized 3D Plots

Plot	**Length (inches)**	**Width (inches)**	**Height (inches)**	**Drag surface area (in^2)**
1	0.5883	0.25	0.1875	0.3125
1	0.5	0.333	0.1875	0.3125
2	0.8333	0.5	0.1875	0.5
2	1	0.333	0.1875	0.5
3	0.333	0.25	0.1875	0.21875

4.2.4.6.1 Settling Prediction Results

Table 10 shows the average settling velocities compared with the settling velocity range of the original data points, and predicted settling velocities using Equation 20. Because previous figures for aluminum showed that drag surface area was not a strong predictor of settling velocity, the custom bar results were simplified into 2-dimensional representations of height and settling velocity. Figures 49, 50, and 51 show that while the custom aluminum pieces fell within the settling velocities of the original pieces, they did not linearly fit the data set. All of the custom pieces averaged settling velocities that were in the upper range of the original pieces and were for the most part similar to the highest settling velocity pieces. Additionally, Equation 20, which incorporates both height and drag surface area, predicted settling velocities below the observed settling velocity results. As was previously stated, the goal of this exercise was to develop aluminum bar dimensions that would result in settling velocities that fell linearly between the two existing data points for all three plots.

Table 10: Results of custom aluminum bars versus predicted settling velocities

Plot	Observed Average Settling Velocity of Custom Bars (in/s)	Settling Velocity Range of Original Bars (m/s)	Predicted Settling Velocity Values of the aluminum bars based on Empirical Equation 20 (m/s)
1	13.19	9.54-13.92	8.53
1	13.17	9.54-13.92	8.53
2	11.97	9.39-12.64	7.33
2	11.77	9.39-12.64	7.33
3	13.86	10.22-14.14	9.90

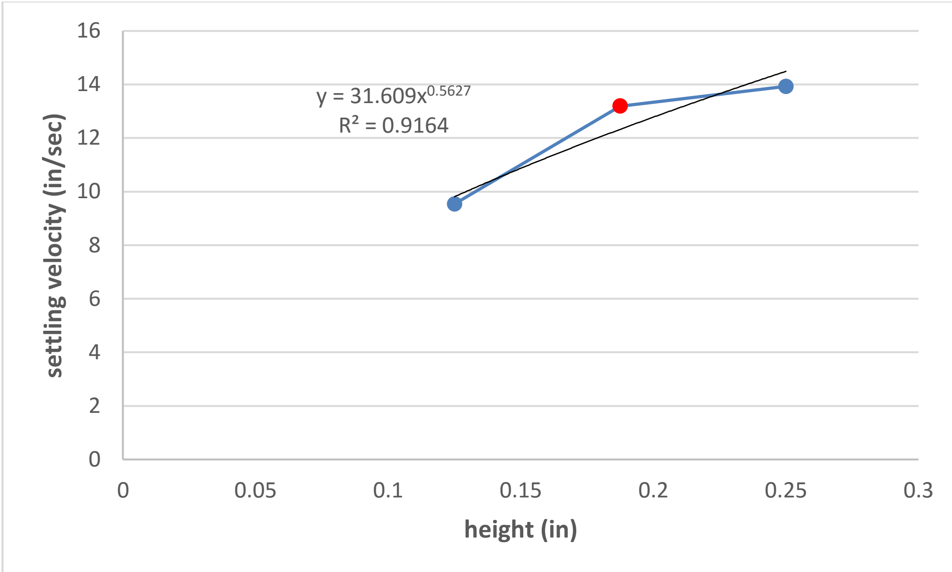

Figure 49: 2-dimensional representation of Figure 47 with addition of results from custom aluminum bars

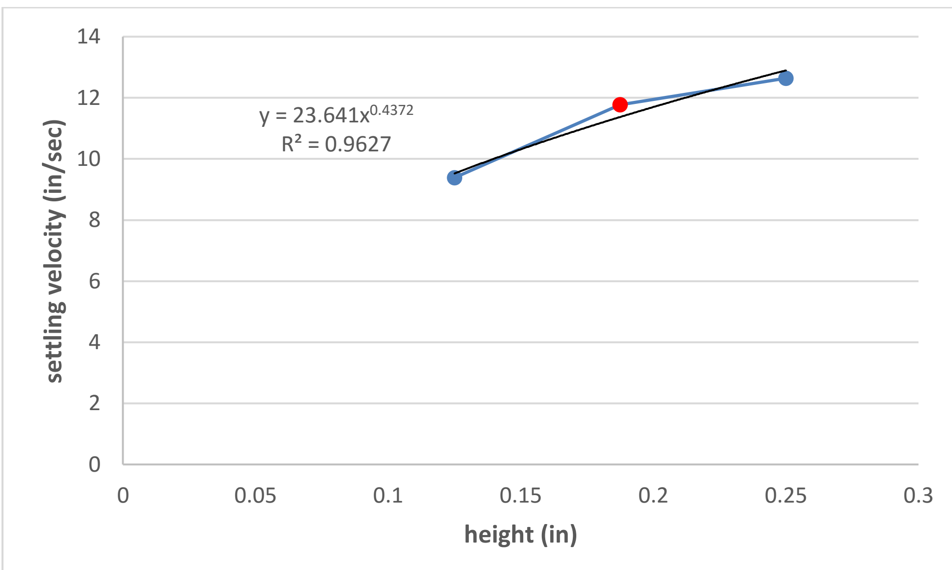

Figure 50: 2-dimensional representation of Figure 48 fitted with custom aluminum bar results

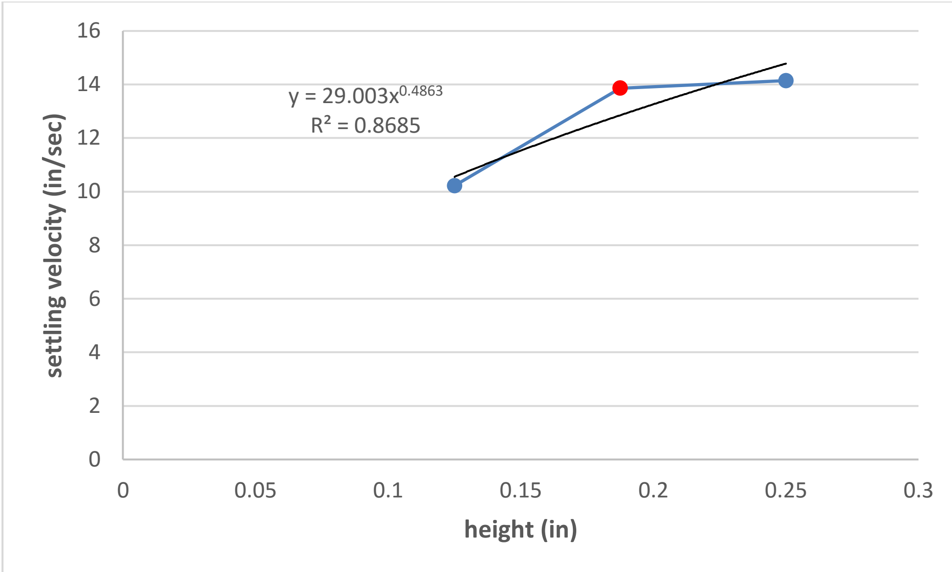

Figure 51: 2-dimensional representation of Figure 49 fitted with custom aluminum bar results

4.3 Aluminum Settling Velocity Model

From Figures 49, 50, and 51, a model was developed to predict the settling velocity for aluminum. The trendline fit for each plot was averaged to develop the model seen in Equation 22

$$\nu = 28.084 * h^{0.4954} \qquad (22)$$

where υ is settling velocity (in/sec), and h is height (in). When tested against the heights for all aluminum bar heights, there was only a 5.6% error overall in the settling velocity prediction. However, when used to predict settling velocity for anthracite, the error was over 100%. Table 11 shows the observed versus calculated settling velocities for all aluminum heights tested. Additionally, Figure 52 shows a strong correlation between the observed settling velocity for all aluminum bars tested and calculated settling velocities using Equation 22 with an R^2 value of 0.91.

Table 11: Observed versus Calculated Settling Velocities for Aluminum Bar Heights

Height (in)	**Observed Settling velocity (in/sec)**	**Calculated settling velocity (in/sec)**	**Percent error**
0.09	9.01	8.69	3.55%
0.125	9.78	10.02	2.45%
0.19	12.13	12.25	0.99%
0.25	13.74	14.13	2.84%
0.38	16.34	17.28	5.75%

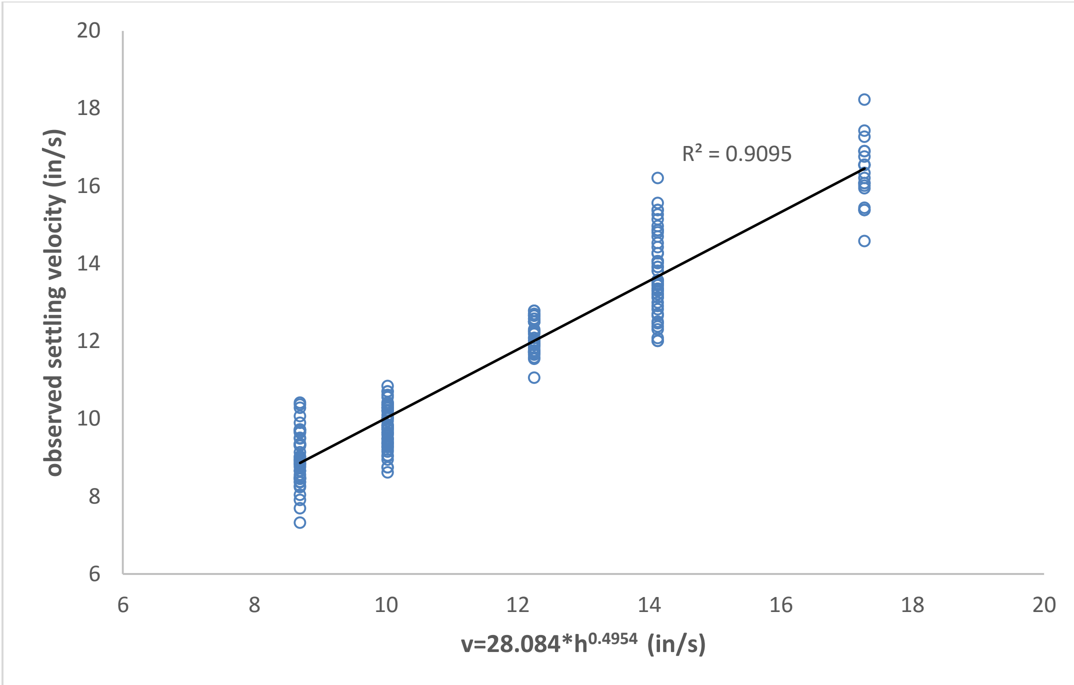

Figure 52: Aluminum observed settling velocity compared with aluminum settling velocity model

4.4 Sieve Analysis Results

4.4.1 Uniformity Coefficient Less than 1.5 Anthracite

Sieve analysis from the top six inches of the 24 inch bed from one of the filter column tests found the d_{10} to be 0.92 mm, d_{60} to be 1.47 mm and uniformity coefficient 1.60 by utilizing the linear correlation equation from the semi-log plot in Figure 53. This is a high uniformity coefficient for what should theoretically be a relatively uniform section of the filter. This result helped to confirm a lack of stratification within the upper section of the filter column.

The sieve analysis of media from the bottom six inches of the same 24 inch column yielded values of 0.98 mm, 1.52 mm and 1.55 for the d_{10}, d_{60} and uniformity coefficient, respectively as determined from Figure 54. The uniformity coefficient for the bottom section of the UC <1.5 media was similar to the top section indicating that there is a uniform distribution throughout the filter column.

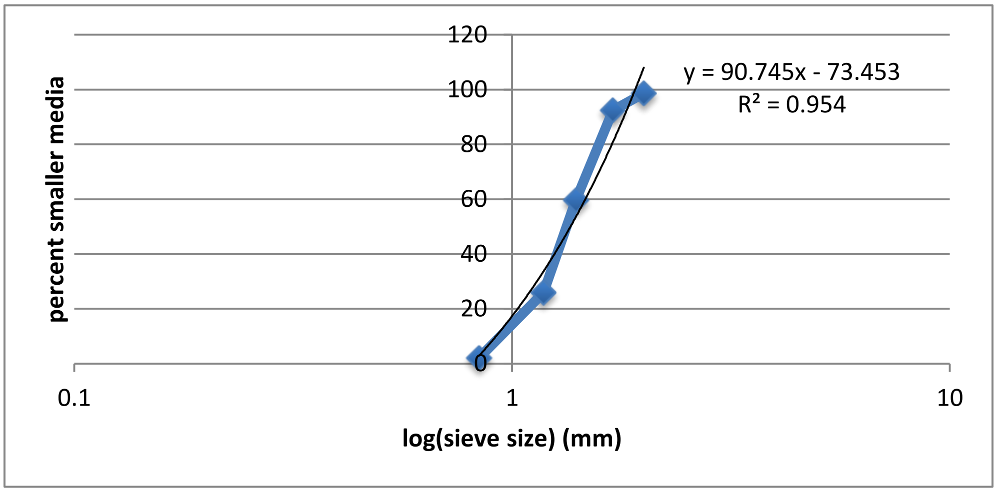

Figure 53: Sieve analysis semi-log plot results from top 6 inches of the filter column

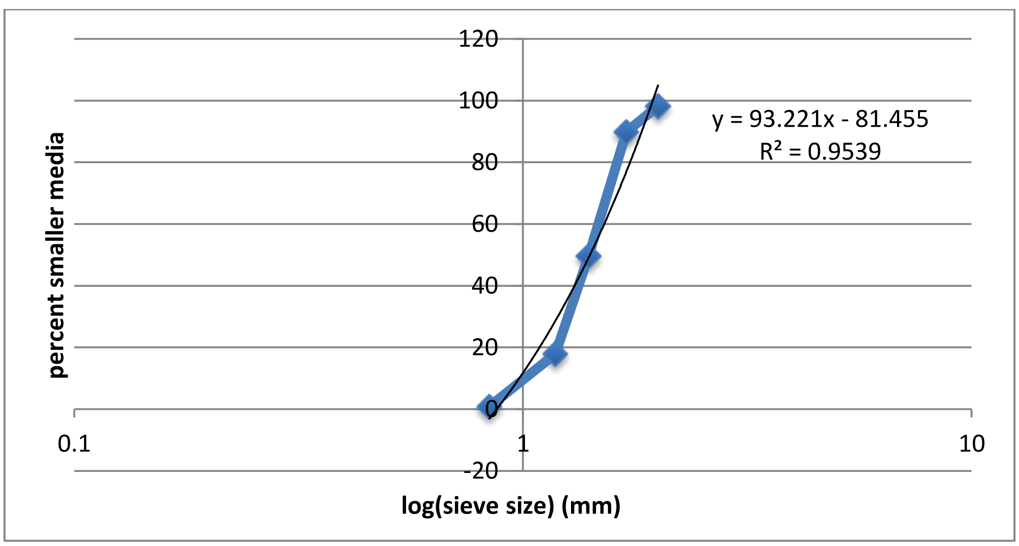

Figure 54: Sieve analysis semi-log plot results from bottom 6 inches of UC <1.5 filter column

4.4.2 Higher Uniformity Coefficient Media

The same sieve analysis was performed on the top six inches of the UC <1.6 media filter column. Results from that sieve analysis yielded a d_{10} of 0.95 mm, a d_{60} of 1.63 mm and a uniformity coefficient of 1.74 (Figure 55). This is a high uniformity coefficient and exceeded the uniformity coefficient of the entire bed by 8%. These results indicate that there is a lack of stratification of the media in the bed and that there is a large difference in media sizes found within the top six inches of this filter column.

For the bottom six inches of the UC <1.6 media, sieve analysis resulted in d_{10}, d_{60} and uniformity coefficient of 1.11 mm, 2.02 mm and 1.81 respectively determined from Figure 56. Again, the uniformity coefficient for the bottom section of the UC <1.6 media was higher than the raw media sieve values.

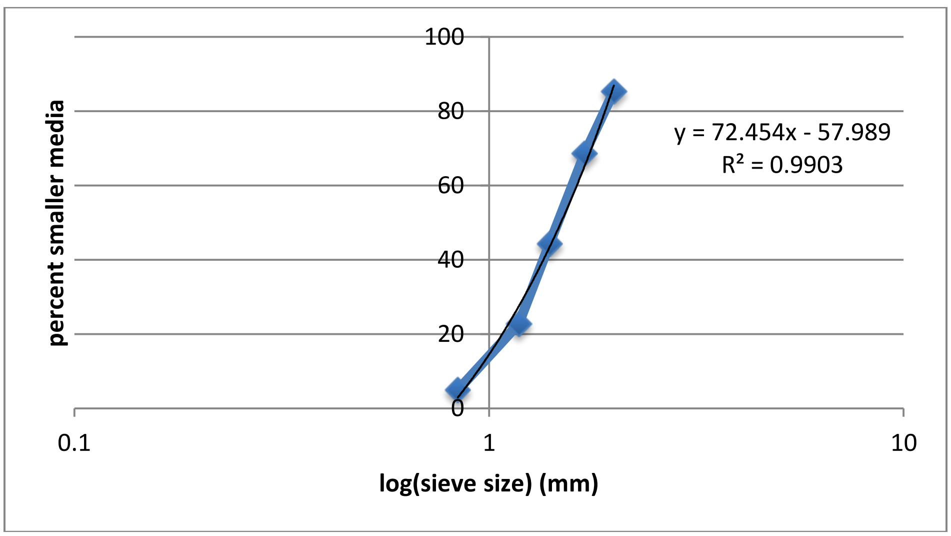

Figure 55: Sieve analysis semi-log plot results from top 6 inches of UC <1.6 filter

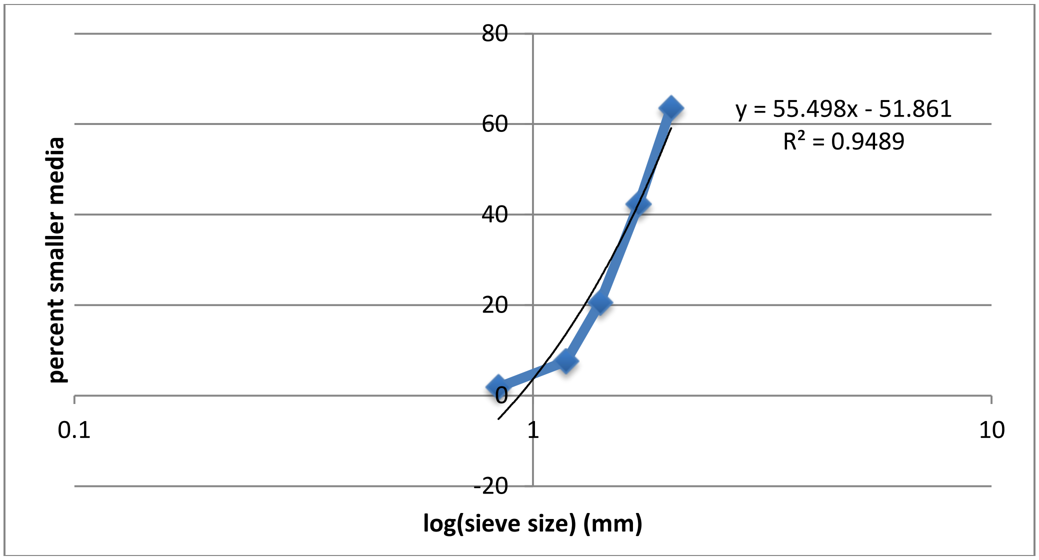

Figure 56: Sieve analysis semi-log plot results from the bottom 6 inches of UC <1.6 filter column

4.4.3 Settling Velocity of Sieved Media

To further analyze the sieved media, the settling velocity of media on the 10 and 14 mesh pans (2.00 mm and 1.41 mm) were tested for both the top and bottom sections of the UC <1.6 media. These pans were selected as they were far enough apart from each other to show a comparison in settling velocities as well as retaining sufficient amounts of media for testing.

Figures 57 and Figure 58 show that there is little difference between the settling velocities of media that fell on the 10 and 14 mesh pans. The theory of sieve analysis would indicate that the settling velocities would differ from pan to pan as particles become smaller through the sieve column. The similar average velocities and large standard deviations that have been seen throughout this research indicate that once again, size is not an indicator of settling velocity or stratification. However, based on t-Test results there does appear to be a difference with P values of 0.0003 for both Figure 57 and Figure 58 which compare settling velocities between the 2.00 mm and 1.41 mm sieve size media for the top and bottom of the filter column. While some of the media clearly does stratify, the degree of stratification is relatively low with both the top and bottom 6 inch sections showing 17% stratification (Figures 59 and 60).

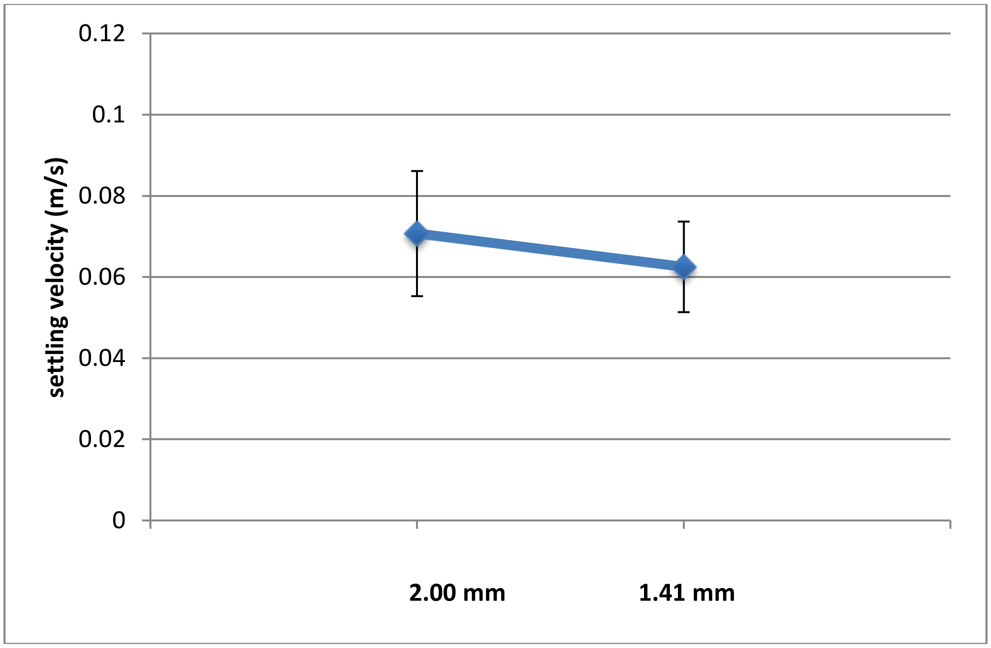

Figure 57: settling velocity average values and standard deviations from 2.00 mm and 1.41 mm media from the top 6 inches of the UC <1.6 filter column

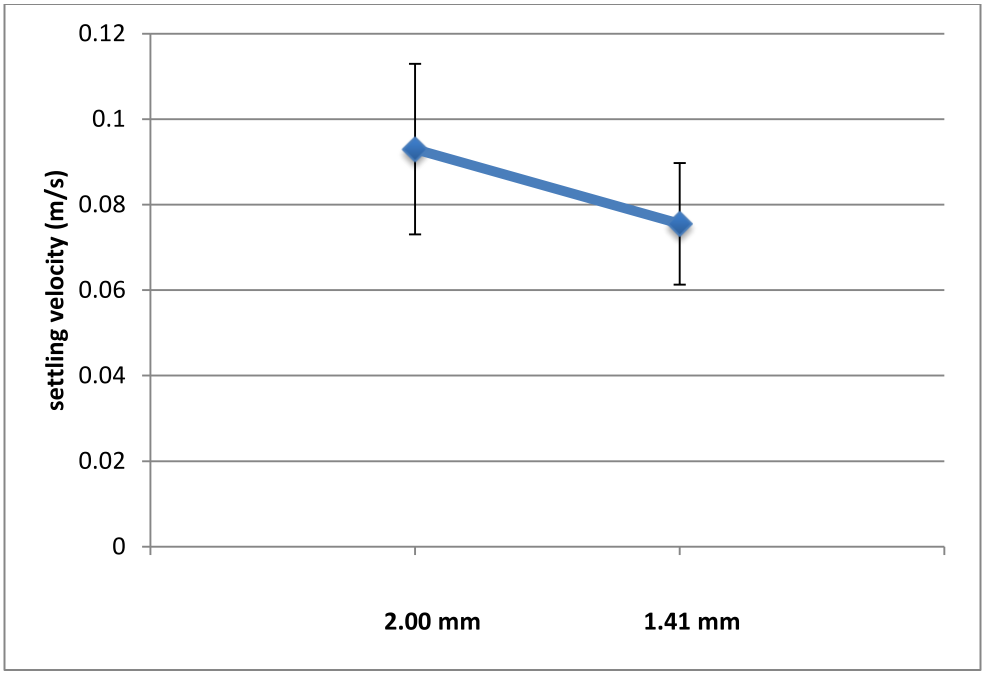

Figure 58: settling velocity average values and standard deviations from 10 and 14 mesh media from the bottom 6 inches of the UC <1.6 filter column

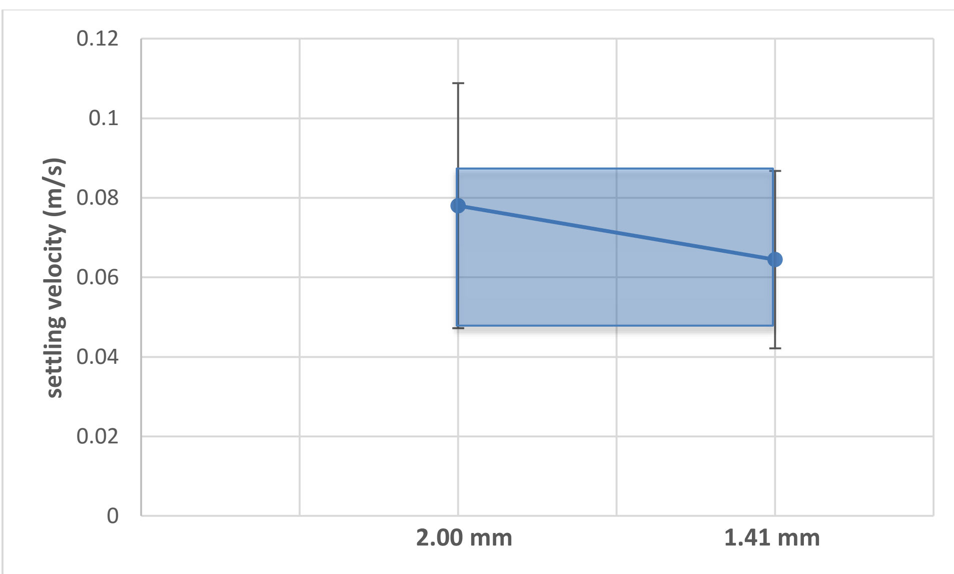

Figure 59: Stratification diagram of the top 6 inches of the UC <1.6 filter column

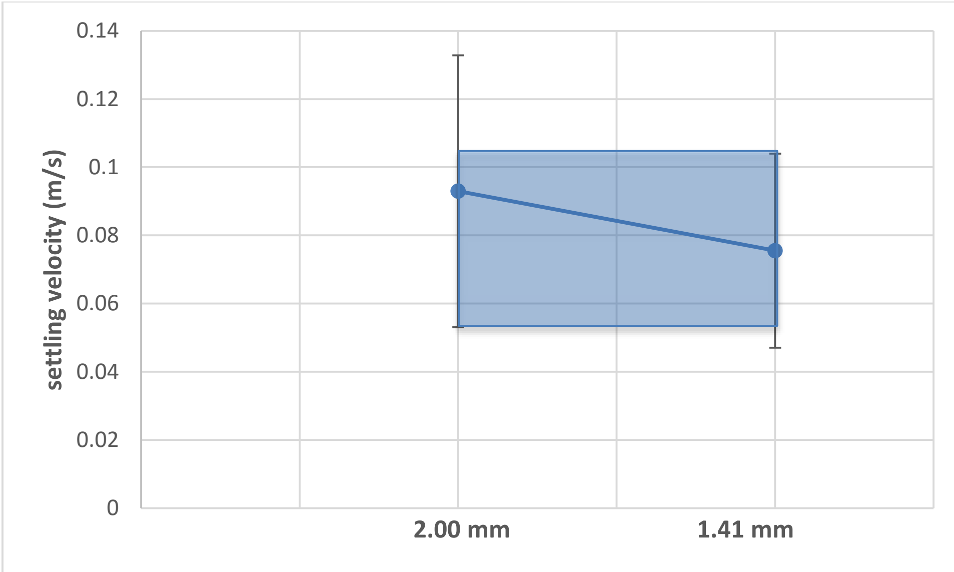

Figure 60: Stratification diagram of the bottom 6 inches of the UC <1.6 filter column

Both the 2.00 mm and 1.41 mm media show a slight difference in settling velocity between the top and the bottom sections of the filter with large standard deviations as seen in Figures 61 and 62. This would indicate that sieve analysis results such as d_{10} size and uniformity coefficient are not strong indicators of settling velocity within a filter and further strengthen the case against using a shape factor. Additionally, t-Tests found significant difference between both the 2.00mm and 1.41mm comparisons with P values of 0.0020 and 0.0017 respectively.

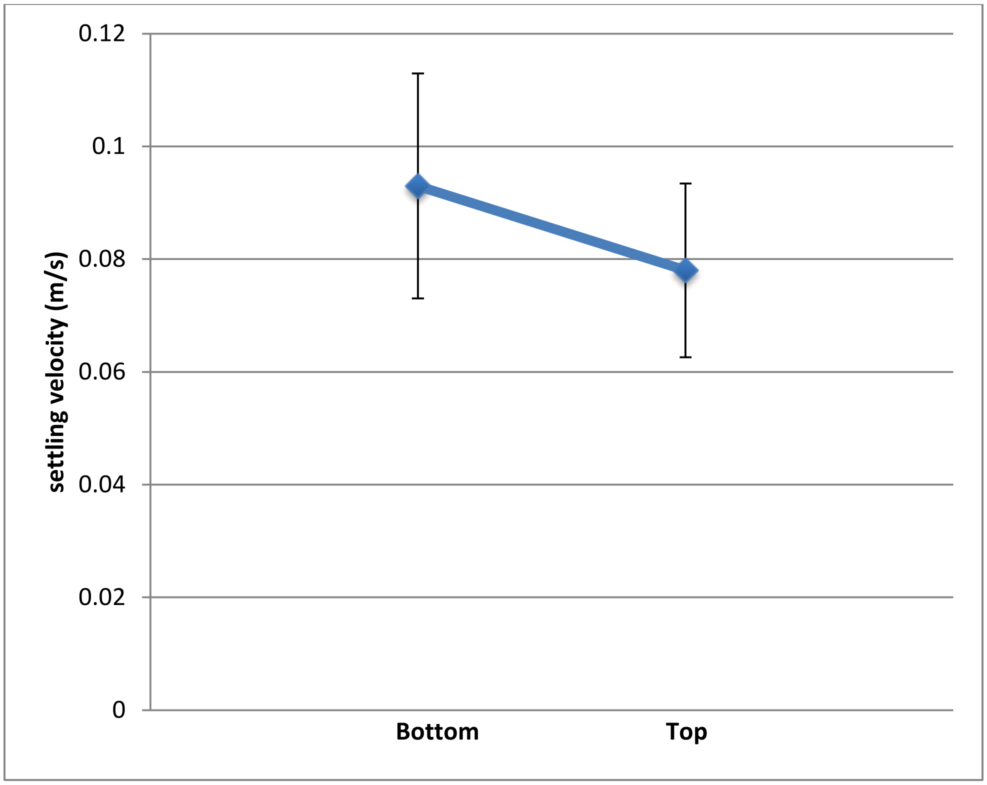

Figure 61: settling velocity average values and standard deviations for 2.00 mm media for top and bottom sections of the UC <1.6 filter column

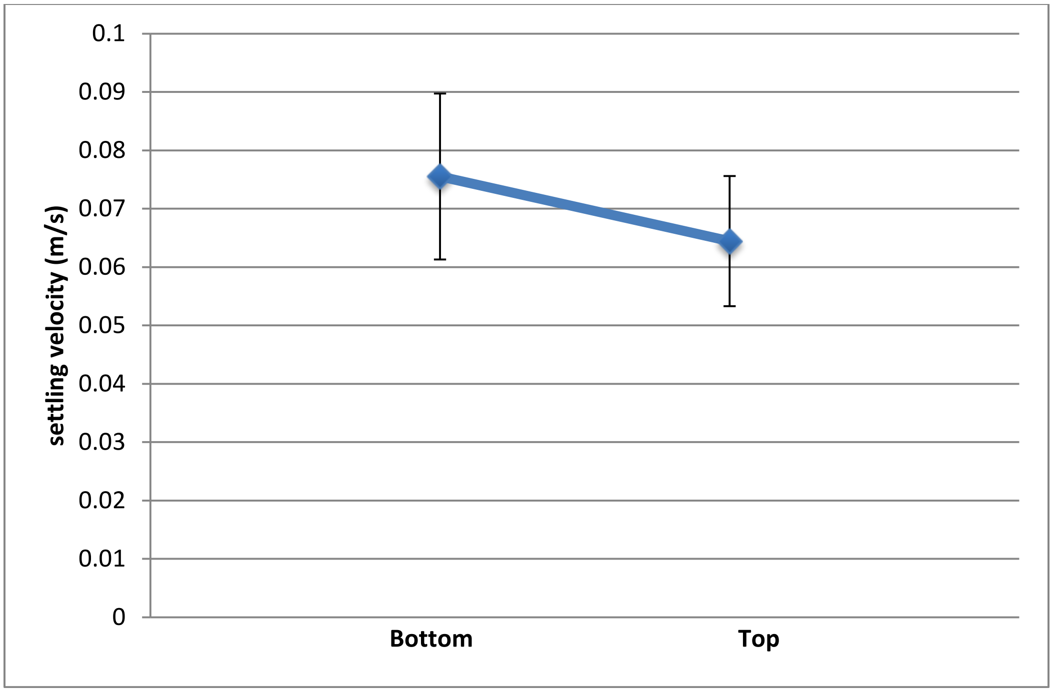

Figure 62: settling velocity average values and standard deviations of 1.41 mm media for the bottom and top sections of the UC <1.6 filter column

4.4.4 Shape Factor Analysis of Sieved Media

4.4.4.1 Smallest Dimension Analysis

Based on previous data, the smallest dimension shows a correlation with settling velocity. In looking at Figures 63 and 64, while average values remain similar for the same mesh, again large standard deviations can be seen. T-Test results for both Figures 63 and 64 confirmed the null hypothesis.

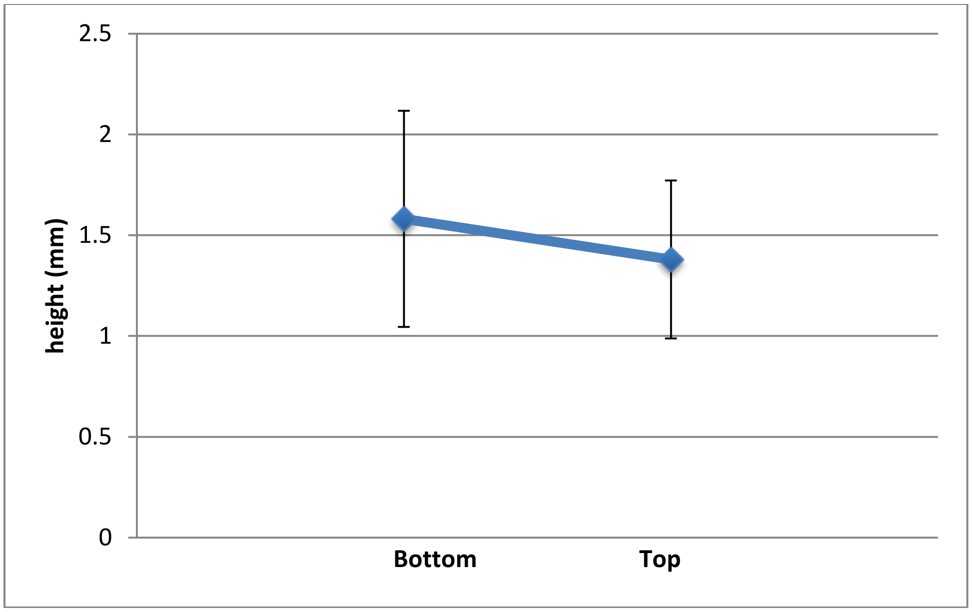

Figure 63: 10 mesh (2.00 mm sieve size) average values and standard deviations of height from the bottom and top sections of the UC <1.6 filter column

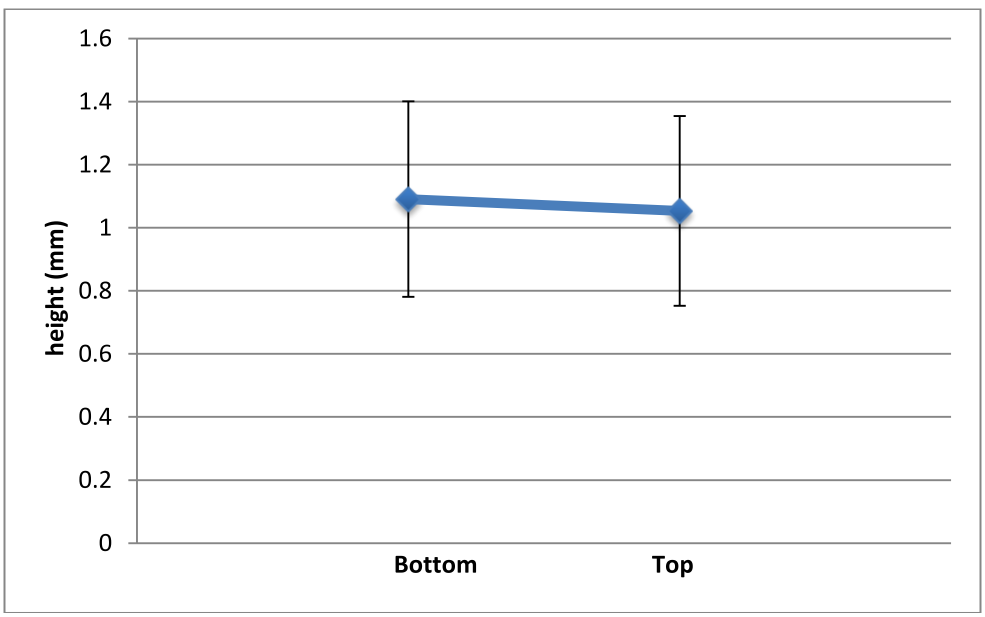

Figure 64: 14 mesh (1.41 mm sieve size) average values and standard deviations of height from the bottom and top sections of the UC <1.6 filter column

4.4.4.2 Drag Surface Area Analysis

The drag surface area calculated is a rough estimate for the anthracite particles given that they are not regularly shaped. The drag surface area was calculated based on rectangular dimensions of length, width and height as calculated for the aluminum bars. Therefore, there is a margin of error in drag surface area calculations of Figures 65 and 66, however they do help in understanding the role of shape factor. While there are large standard deviations shown, particularly for the 10 mesh (2.00 mm sieve size), there is a clear stratification of drag surface area between the top and the bottom sections of the filter. This helps to show that while the particles may not be stratifying based on settling velocity, they are stratifying in a manner that is more based on a shape factor. As previously noted, drag surface area is determined by the shape and dimensions of a particle. A change in height has a more significant change over drag surface area than length and width because it is accounted for twice in the calculations. Drag surface area controls the amount of drag surrounding a particle as it is settling. A t-Test confirms a significant difference in populations for both Figures 65 and 66 with P values of <0.0001.

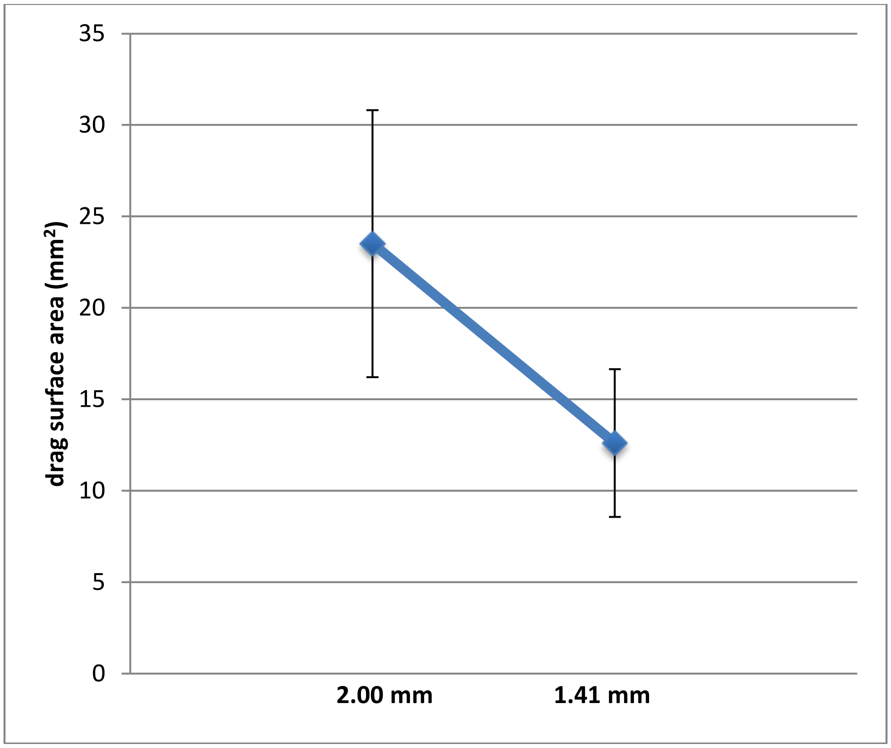

Figure 65: 2.00 mm and 1.41 mm sieve size average values and standard deviations of drag surface area from the top 6 inches of the UC <1.6 filter column

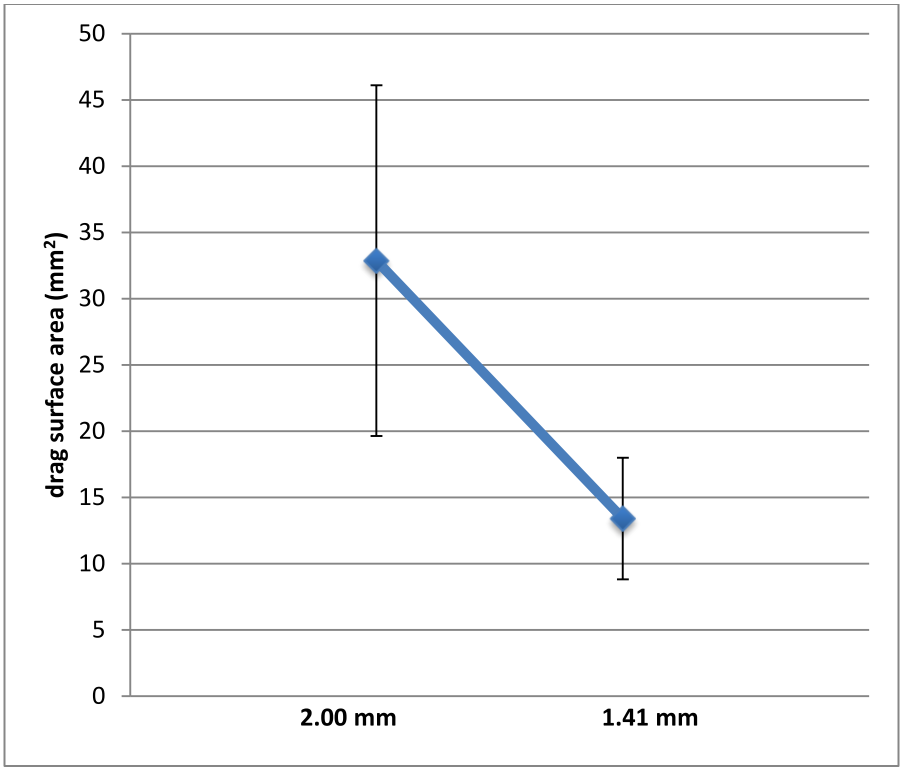

Figure 66: 2.00 mm and 1.41 mm sieve size average values and standard deviations of drag surface area from the bottom 6 inches of the UC <1.6 filter column

4.5 Sand Stratification

A filter column with 18 inches of 0.51 mm effective size sand with a uniformity coefficient of <1.5, and a density of 2.65 g/cm^3 was backwashed to 50% expansion at 28 gpm/ft^2 (69 m/h) for 20 minutes. Figure 67 visibly shows the stratification of sand that resulted after backwashing. These results confirm the literature findings regarding the stratification of sand (Cleasby and Woods, 1975).

Following this experiment, two additional experiments were conducted with the sand to mirror those for anthracite and to confirm the visual stratification of sand seen. The first experiment was with a 2-inch filter column with 24 inches of sand backwashed to 50% expansion for 20 minutes at 30 gpm/ft^2 (73 m/h). After backwashing, the flow was immediately shut-off. Figure 68 shows a distinct upward trend in the settling velocity from the top of the filter to the bottom and a 38% difference in the average settling velocity between the top and bottom of the filter column. Additionally, the standard deviations for each section of the filter are lower than what was seen for anthracite.

An ANOVA statistical test between all populations found a statistically significant difference with a P value <0.0001. Additionally, a statistically significant difference was found between all filter sections except for the two adjacent middle sections. Table 12 shows the complete statistical t-Test data for sand.

To quantify the amount of stratification, the error bars were taken out to ±2 standard deviations to provide a 95% confidence interval. From here, as with anthracite, the number of particles within the overlapping area was compared to the non-overlapping area (Figure 69). It was found that 9% of the sand fell within the overlapping area, while 91% of the sand was “stratified”. The 9% “un-stratified” particles helps to explain why the two middle sections were found to be indifference from one another since the overlap area is defined by the top and bottom sections only.

The second backwash experiment, followed the same procedure, except the flow following backwash was ramped down by 1 gpm/ft^2 every 30 seconds from a max velocity of 25 gpm/ft^2 to 7 gpm/ft^2 when the bed was fixed.

A sieve analysis of each 6 inch filter section was performed for both the ramped and immediate shut-off pump speed. Results from the sieve analysis showed low percent difference between any section, therefore a settling test on the ramped down filter column was not performed. See Table 13 for percent differences between d_{10}, d_{60}, and UC for the two tests.

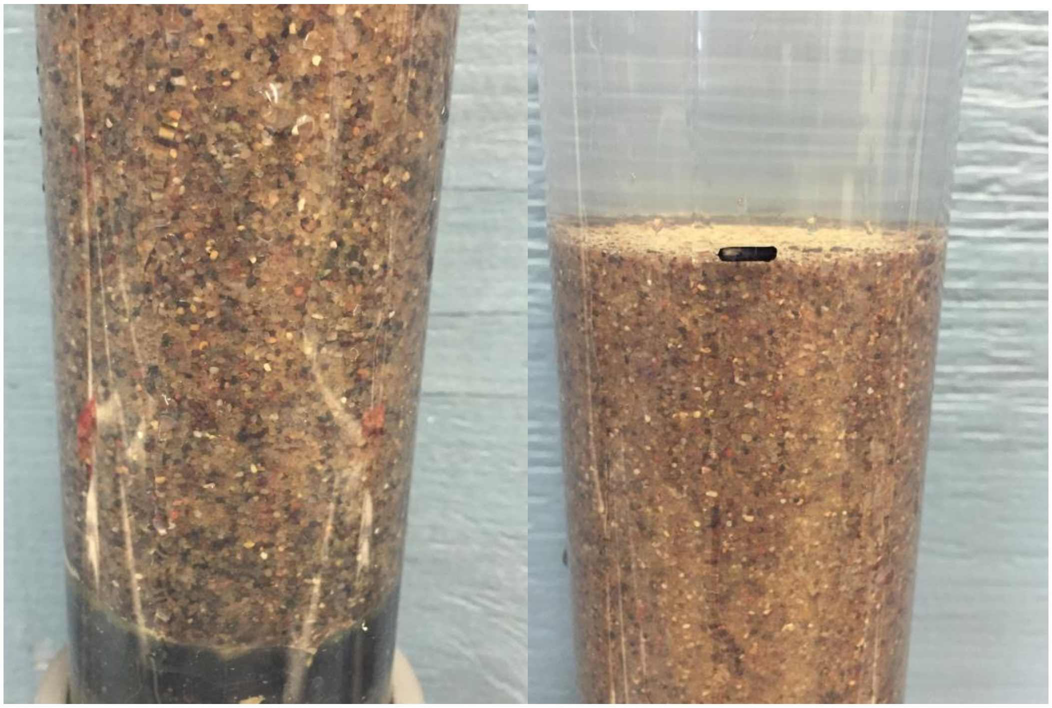

Figure 67: Bottom of filter (left) and top of filter (right) showing visible stratification of sand by size

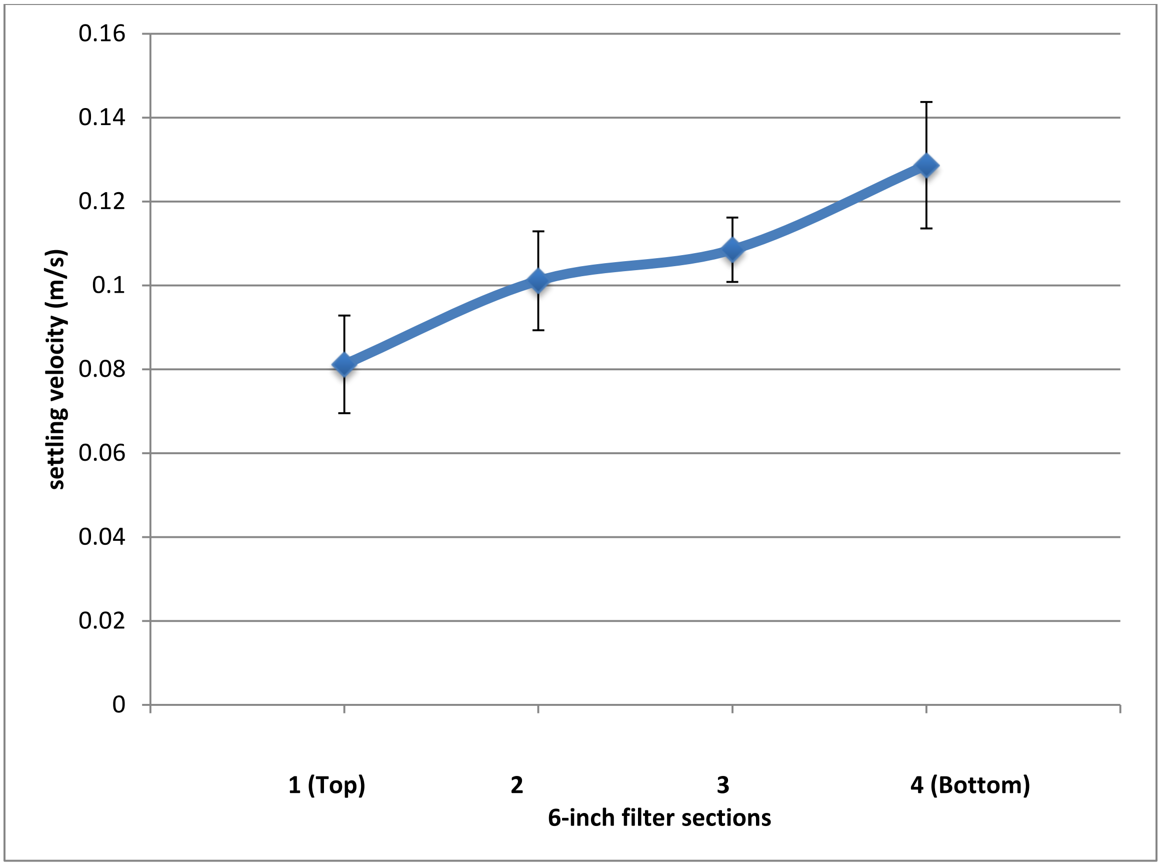

Figure 68: Settling velocity profile of sand from the top of the filter column to the bottom

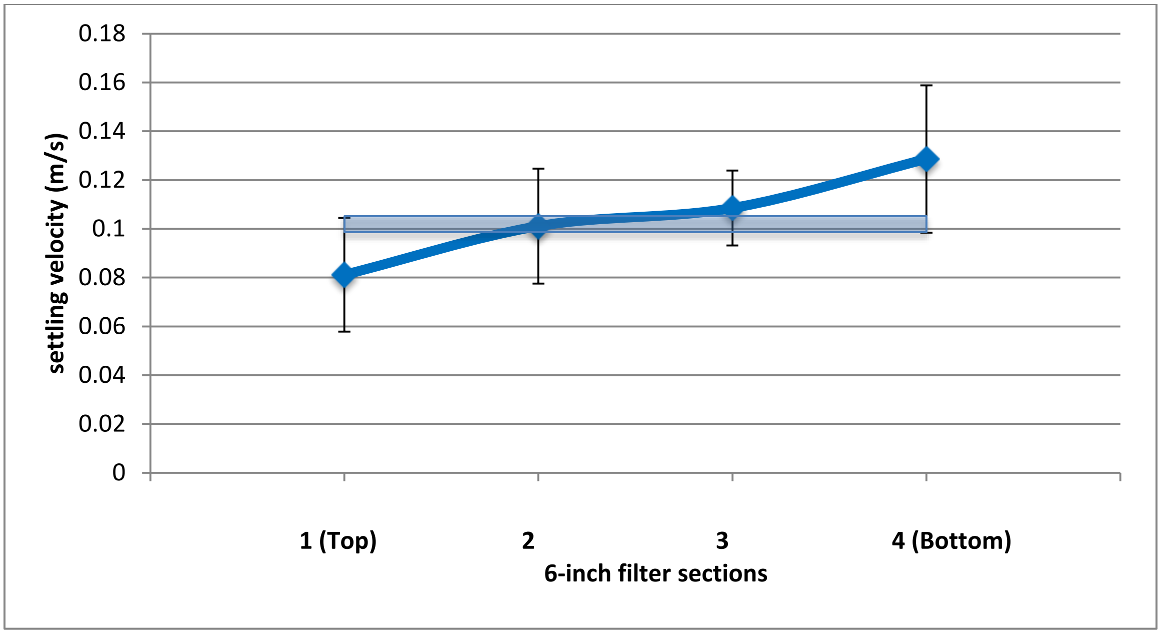

Figure 69: Stratification diagram of sand

Table 12: Statistical t-Test results for sand

Filter Sections	P value comparing settling velocity between filter sections
1 and 2	<0.0001
1 and 3	<0.0001
1 and 4	<0.0001
2 and 3	0.0057
2 and 4	<0.0001
3 and 4	<0.0001

Table 13: Percent difference of filter section effective sizes and uniformity between ramped and unramped pump speed following backwash for sand based on sieve analysis

	d_{10} size percent difference	**d_{60} size percent difference**	**Uniformity Coefficient percent difference**
24 in (Top)	1.15%	5.84%	4.64%
18 in	1.16%	3.05%	1.91%
12 in	6.48%	0.88%	7.87%
6 in (Bottom)	5.95%	4.17%	1.89%

4.6 Minimum Fluidization Velocity

4.6.1 Uniform Anthracite Results

Minimum fluidization velocity was tested using the UC <1.5, 0.94 mm effective size media. Using the 1.7 mm sieve opening size, the minimum fluidization velocity was calculated to be 11.80 gpm/ft^2 (28.4 m/h) assuming a uniformity coefficient of 1. Minimum fluidization, defined as the point where all the media in the bed is visibly fluidized, was observed at approximately 15 gpm/ft^2 (37 m/h). This value is similar to the calculated 1.3*v_{mf} design standard of 15.3 gpm/ft^2 (37.5 m/h). This 27% difference helps indicate that irregularly shaped media does not correlate to sieve sizes. Additionally, this would indicate that the nominal diameter is not an accurate predictor of fluidization velocity in the Wen and Yu model, nor does it correlate to an equivalent sphere diameter for irregularly shaped media grains.

4.6.2 Sand Minimum Fluidization Velocity

The minimum fluidization velocity for sand was calculated at 12 gpm/ft^2 (29m/h). Minimum fluidization velocity was observed at 14 gpm/ft^2 (35 m/h) with a 17% difference between calculated and observed minimum fluidization velocity.

4.7 Sphericity

Sphericity was calculated for anthracite that fell on the 1.4mm and 2.00mm sieve pans and was used to compare observed settling velocity to calculated settling velocity. The average sphericity for anthracite was calculated to be 0.43. Using equations 12, 13, and 14, the calculated settling velocities for the 1.4 mm and 2.00 mm anthracite was 0.096 m/s and 0.14 m/s respectively. Compared against observed settling velocities, there was a 39% average error for the 2.00 mm anthracite and a 27% average error for the 1.4 mm anthracite (Table 14). This indicates that sphericity does not provide very accurate values for the prediction of settling velocity as sieve size does not equate to an equivalent sphere diameter for anthracite with a 57% difference seen between sieve size diameter and calculated equivalent sphere diameter. Additionally, the surface area of irregularly shaped media is difficult to measure accurately adding an unknown level of error to calculations.

Table 14: Comparison of measured and calculated settling velocities

Media Sieve Size (diameter)	**Equivalent sphere diameter**	**Average Observed Settling Velocity**	**Calculated Settling Velocity**	**Percent Difference**
1.4 mm	0.6 mm	0.070 m/s	0.096 m/s	27%
2.00 mm	0.86 mm	0.085 m/s	0.14 m/s	39%

4.8 Low Density Anthracite and Ceramic

Ceraflow-50, a spherical non-expanded ceramic media, which has an effective size of 0.28 mm and a uniformity coefficient of 1.26 and a 0.8 mm effective size anthracite were used in this experiment. Effective sizes and uniformity coefficients were determined through sieve analysis.

The backwash velocity at 50% expansion was 9.8 gpm/ft^2 (24 m/h) for the dual media bed. Following backwash, the media was allowed to settle and as predicted, there was a distinct interface between the anthracite and ceramic layer with minimal intermixing observed (Figure 70). Minimum fluidization velocity was calculated at 1.03 gpm/ft^2 (2.53 m/h) and 6.34 gpm/ft^2 (15.5 m/h) for ceramic and anthracite respectively using the Wen and Yu minimum fluidization equation at 20ºC. The ceramic fluidized at approximately 2.7 gpm/ft^2 (6.8 m/h), and the anthracite fluidized at approximately 7.3 gpm/ft^2 (18 m/h). This equates to a 162% difference for the ceramic and a 15% difference for the anthracite indicating that the Wen and Yu equation may not be an accurate prediction tool for ceramic media. Additionally, the 63% difference in minimum fluidization rates help to explain why these two media remain stratified following backwash.

Figure 70: Low density anthracite and ceramic filter column stratification post-backwash

CHAPTER 5: CONCLUSIONS

The following conclusions were drawn based on the results of this research study:

Rectangular aluminum bars with height dimensions ranging from 3/32” to 3/8”were used to establish the relationship between height and settling velocity in a water column with an R^2 value of 0.90. Additionally, changes in length and width did not result in significant changes in settling velocity. The height (or smallest dimension) was also found to be significant in the prediction of settling velocity for anthracite with a d_{10} (effective size) of 0.95-1.10 mm, and height typically between 0.2-1.6 mm. A correlation (R^2 of 0.50) was found between the settling velocity and height for anthracite.

The drag surface area was also found to have influence on the settling velocity of anthracite with an R^2 value of 0.35. Although changes in length and width also result in changes to drag surface area, minimal change was seen in the settling velocity.

Sand visibly stratifies by size with smallest sand grains on the top and largest sand grains settling to the bottom of the filter. This was confirmed by settling testing and sieve analysis with 91% of the sand grains classified as stratified and a 38% difference between the average settling velocity of the top and bottom of the filter column.

Anthracite does not stratify to the degree that sand does. While sand showed 91% stratification, anthracite showed only 9-15% stratification in similar experiments. Additionally, anthracite only showed a 14% difference between the average settling velocity of the top and bottom of the filter column versus a 38% difference for sand.

Sieve analysis also showed that sections of an anthracite filter column are not stratified by size with uniformity coefficients of the top and bottom sections of the media remaining very similar to the uniformity coefficient of the entire bed.

A model was developed to predict the settling velocity of the anthracite (Equation 18).

$$v\left(\frac{m}{s}\right) = \frac{h^2}{A_{drag}} \qquad (18)$$

A 36% error was seen when compared to observed settling velocity values for anthracite. Because of the irregular shape of the anthracite, it is much more difficult to accurately measure and model than more uniform and spherical sand. The model for the anthracite was developed with the assumption that the anthracite particles were rectangular in shape since it was not possible to account for the shape irregularity of each grain. In comparison, a model was developed for the rectangular aluminum bars (Equation 21) with only 5% error due to more uniform shape and precise measurements.

$$v = 28 * h^{0.5} \qquad (21)$$

CHAPTER 6: FUTURE RECOMMENDATIONS

For future studies, additional research into the irregular shape of media grains should be taken into consideration. This will allow for greater accuracy in the determination of shape factor and controlling dimensions. Additionally, there should be greater research into the accuracy of sieve analysis for non-spherical media and how these differences affect settling velocity predictions and stratification. The Wen and Yu minimum fluidization velocity equation should be analyzed against media sizes determined through sieve analysis.

Other ideally shaped particles should be tested to confirm the controlling variables determined in this research study. This could include ellipsoidal, cubic, and multi-surface shaped particles. Modeling particles that more closely resemble the shape and density of actual filter media would be useful for comparison. In this study Reynolds number and drag coefficient were not thoroughly studied. Future research should incorporate these variables for comparison against controlling dimensions.

For the theory surrounding shape factor to advance, it is necessary to develop a model that will accurately incorporate shape factor into settling velocity prediction equations. The initial objective of this research study was to better understand the mechanics of anthracite in a filter in order to add a less dense ceramic layer above it. Because research objectives changed, this was not carried forth. Future research should build upon the research of this study to identify ways to optimize filter performance through the addition of larger, less dense media above the anthracite without significant intermixing through the development of a shape factor model for accurate settling velocity prediction.

Finally, as this research has shown shape to be significant in the stratification of anthracite, influences of shape on expanded ceramic should also be studied.

REFERENCES

Amburgey, J.E. (2005). Optimization of the extended terminal subfluidization wash (ETSW) filter backwashing procedure. Water Resarch, 39(2), 314-330.

Amburgey, J. E., & Brouckaert, B. M. (2012). AWWA WQTC Conference. In *The Use of Expanded Clay Media to Extend Run Times in Existing Dual-Media Filters*. American Water Works Association.

Amirtharajah, A., & Cleasby, J. L. (1972). Predicting Expansion of Filters During Backwash. American Water Works Association, 64(1), 52-59.

ASTM C128-12, Standard Test Method for Density, Relative Density (Specific Gravity), and Absorption of Fine Aggregate, ASTM International, West Conshohocken, PA, 2012, www.astm.org

ASTM C136-06, Standard Test Method for Sieve Analysis of Fine and Coarse Aggregates, ASTM International, West Conshohocken, PA, 2006, www.astm.org

Baba, J., & Komar, P. D. (1981). Settling Velocities of Irregular Grains at Low Reynolds Numbers. SEPM Journal of Sedimentary Research SEPM JSR, Vol. 51.

Baldock, T., Tomkins, M., Nielsen, P., & Hughes, M. (2004). Settling Velocity of Sediments at High Concentrations. Coastal Engineering, 51(1), 91-100.

Cleasby, J., Arboleda, J., Burns, D., Prendiville, P., & Savage, E. (1977). Backwashing of Granular Filters. American Water Works Association, 69(2), 115-126.

Cleasby, J. L., & Woods, C. F. (1975). Intermixing of Dual Media and Multimedia Granular Filters. American Water Works Association, 67(4), 197-203.

Conley, W. R., & Camp, T. R. (1961). Experience with anthracite-sand filters [with discussion]. *American Water Works Association, 53*(12), 1473-1483.

Conley, W. R., & Hsiung, K. (1969). Design and application of multimedia filters. *American Water Works Association, 61*(2), 97-101.

Crittenden, J. C. (2012). MWH's Water Treatment: Principles and Design (3rd ed.). Hoboken, NJ: John Wiley & Sons.

Dietrich, W. E. (1982). Settling Velocity of Natural Particles. Water Resources Research Water Resour. Res., 18(6), 1615-1626.

Epstein, N., & Pruden, B. (1999). Liquid fluidisation of binary particle mixtures—III Stratification by size and related topics. *Chemical Engineering Science, 54*(3), 401-415.

Escudié, R., Epstein, N., Grace, J., & Bi, H. (2006). Effect of particle shape on liquid fluidized beds of binary (and ternary) solids mixtures: Segregation vs. mixing. *Chemical Engineering Science, 61*(5), 1528-1539.

French, D. (2012). Granular filter media: Evaluating filter bed depth to grain size ratio. *Filtration Separation, 49*(5), 34-36.

Gabitto, J., & Tsouris, C. (2008). Drag coefficient and settling velocity for particles of cylindrical shape. Powder Technology, 183(2), 314-322.

Goldbery, R., & Richardson, D. (1989). The Influence of Bulk Shape Factors on Settling Velocities of Natural Sand-sized Sedimentary Suites. Sedimentology, 36(1), 125-136.

Hudson, H. E., Jr. (1938). Filter materials, filter runs and water quality. *American Water Works Association, 30*(12), 1992-2009.

Kawamura, S. (1999). Design and operation of high-rate filters. *American Water Works Association, 91*(12), 77-90.

Kawamura, S. (1975). Design and operation of high-rate filters- part 1. *American Water Works Association, 67*(10), 535-544.

Komar, P. D., & Reimers, C. E. (1978). Grain Shape Effects on Settling Rates. The Journal of Geology, 86(2), 193-209.

Richardson, J. F., & Zaki, W. N. (1954). The sedimentation of a suspension of uniform spheres under conditions of viscous flow. *Chemical Engineering Science, 3*,2, 65-73.

Tassitino, M. (2014). *Backwash and Fluidization of Ceramic Media in Multimedia Granular Filters for Water Treatment* (Master's thesis, University of North Carolina at Charlotte) (pp. 1-126). ProQuest.

Tomkins, M. R., Baldock, T. E., & Nielsen, P. (2005). Hindered settling of sand grains. *Sedimentology, 52*(6), 1425-1432.

Vigneswaran, S., & Mazumdar, B. (1984). Intermixing of media in dual media filters. Effluent and Water Treatment Journal, 341-345.

Wadell, H. (1932). Volume, Shape, and Roundness of Rock Particles. The Journal of Geology, 40(5), 443-451.

APPENDIX A: SIEVE ANALYSIS RESULTS

Table A1: Uniformity Coefficient Less Than 1.6 Anthracite

Sample size = 100g						
Mesh #	Opening (mm)	log	Weight media	% retained	% retained sum	% finer
10	2	0.301029996	24.34	24.34	24.34	75.66
12	1.7	0.230448921	20.33	20.33	44.67	55.33
14	1.4	0.146128036	24.17	24.17	68.84	31.16
16	1.18	0.071882007	16.69	16.69	85.53	14.47
Pan			12.98	12.98	98.51	1.49

d_{10}= 1.10mm
d_{60}= 1.80mm
UC= <1.6

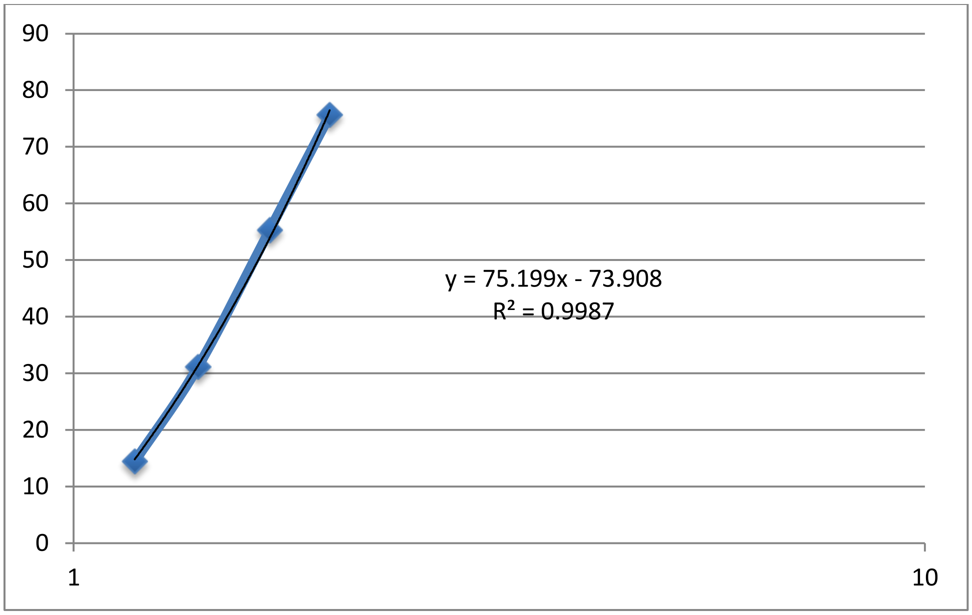

Figure A1: UC <1.6 Semi-Log Plot

Table A2: Uniformity Coefficient Less Than 1.5 Anthracite

sample size= 100g							
mesh#	opening (mm)	initial mass pan	mass pan + mass retained	mass retained	% retained	% sum	% finer
10	2	440.5	441.7	1.2	0.012	0.012	98.8
12	1.7	441.6	448.1	6.5	0.065	0.077	92.3
14	1.4	428	464.9	36.9	0.369	0.446	55.4
16	1.18	418.8	451.6	32.8	0.328	0.774	22.6
20	0.841	402.4	423.6	21.2	0.212	0.986	1.4
pan	0	355	356.7	1.7	0.017	1.003	0

d_{10}= 0.95mm
d_{60}= 1.49mm
UC= <1.5

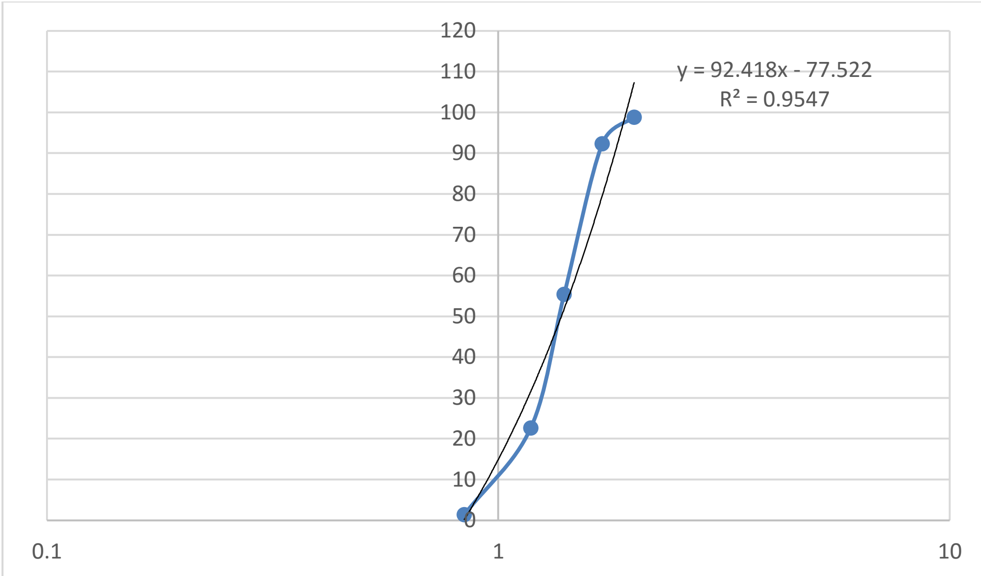

Figure A2: UC <1.5 Semi-Log Plot

Table A3: Sand

sample size= 100g							
mesh#	opening (mm)	initial mass pan	mass pan + mass retained	mass retained	% retained	% sum	% finer
20	0.85	402.4	420.2	17.8	0.178	0.178	82.2
30	0.6	392.1	458.5	66.4	0.664	0.842	15.8
35	0.5	370.4	381.6	11.2	0.112	0.954	4.6
40	0.425	365.4	368.6	3.2	0.032	0.986	1.4
pan		355.1	356.3	1.2	0.012	0.998	0.2

d_{10}= 0.51mm
d_{60}= 0.76mm
UC= <1.5

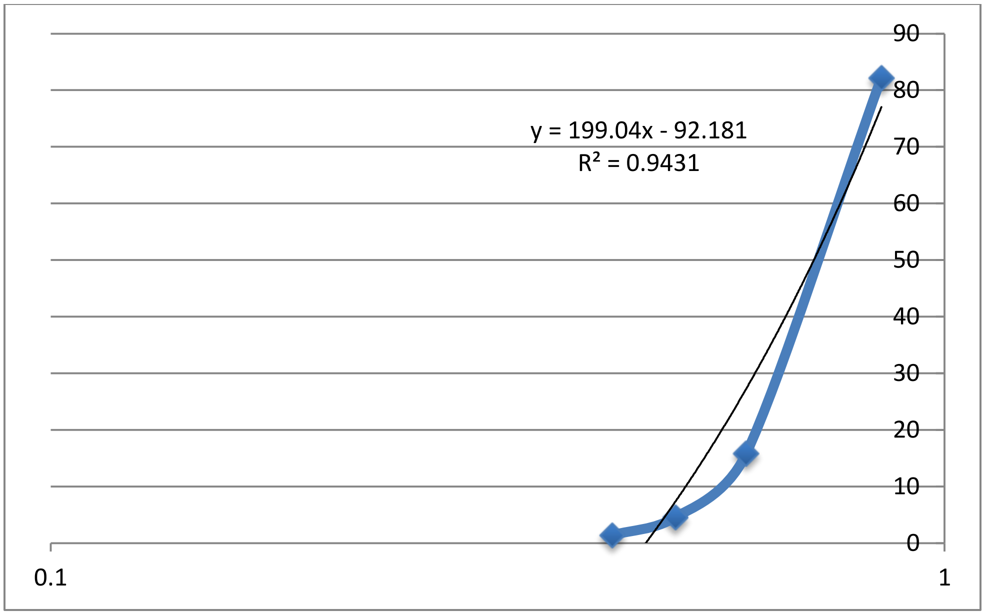

Figure A3: Sand Semi-Log Plot